Applied Ocean Research 97 (2020) 102090

Contents lists available at ScienceDirect

Applied Ocean Research

journal homepage: www.elsevier.com/locate/apor

Experimental studies of a damaged ship section in beam sea waves

M.A. Siddiqui[a,*], M. Greco[a,b], C. Lugni[a,b], O.M. Faltinsen[a]

[a] Centre for Autonomous Marine Operations and Systems (NTNU AMOS), Department of Marine Technology, NTNU, Trondheim, Norway
[b] CNR-INM, Institute of Marine Engineering, Via di Vallerano 139, 00128 Roma, Italy

ARTICLE INFO

Keywords:
2d ship model experiments
Damaged ship raos
Sloshing & piston mode resonance
Ship transient flooding

ABSTRACT

This work presents a series of experiments performed with a prismatic hull form in a small wave flume. The model is a midship section with rectangular damage opening on the side. It is slightly smaller than the flume breadth to achieve predominantly two-dimensional behavior in the experiments. Freely-floating tests in regular beam-sea waves have been carried out on the model section in intact and damaged conditions. Free-roll decay tests were performed for intact and damaged sections to understand the effect of floodwater on roll natural period and roll damping of the model. Video recordings and measurements of wave elevation inside the damaged compartment were performed in all experiments. Linear response amplitude operators (RAOs) for water elevation inside the model and model motions are presented and discussed. Effect of wave steepness, wave period, initial loading condition, damage-compartment division about centerplane (symmetric/asymmetric flooding), damage-opening size and air compressibility in the damaged compartment are examined. The presented results demonstrate occurrence of sloshing and piston mode resonances and their influence on damaged ship motions in waves is highlighted. A linearized strip theory method based on viscous flow is implemented to cross-check and complement the experimental results. The latter method can estimate the damaged ship motions with reasonable accuracy. The initial loading condition determines the equilibrium flooding state and, therefore, the sloshing and piston mode resonance frequencies of the flooded water. The damage-opening size mainly affects the roll damping behavior of the section. Air compressibility in the airtight compartment acts as a coupled spring system with the floodwater and restricts the free-surface motion in the damaged compartment. Cases of transient flooding for a damaged section are also presented, where the freely floating model moves in beam-sea waves and subsequent flooding takes place. Effect of wave steepness, incident wave period and initial intact stability of the model is examined for this scenario. The present work is a continuation of a series of experiments conducted on the same damaged section for forced heave motions documented in [1]. Due to the complex and nonlinear behavior of floodwater inside a damaged ship section, as the previous analysis, the current work is aimed to contribute in the physical understanding of ship behavior in damaged conditions, as well as to serve as a database for the research community to be used for numerical validation.

1. Introduction

Flooding in ships is a complex phenomenon often resulting from damage due to collision, grounding or rough weather. A large number of ship collisions in recent years have led to loss of lives, and hazardous cargo spills/loss. Behavior of a flooded ship differs significantly from an intact condition. Floodwater enters through the damaged opening, leading to loss of stability, excessive heel or trim and in some cases capsizing. Over the past few decades, accidents like the European Gateway (1982), Herald of the Free Enterprise (1987), Estonia (1994), MV Sewol (2014), as well as more recent damages to oil tankers and other similar capsizes leading to catastrophic loss of lives and property, have inspired many researchers to study ship flooding and its effect on ship motions. Roll On/Roll Off (RO-RO) ferries, which are nowadays important means of transportation on short sea routes, can suffer greatly the occurrence of flooding. In fact, these ships have large decks with no vertical bulkheads in car decks to be able to fit a large number of vehicles. This can cause a relevant free-surface effect due to floodwater and loss in static stability even with a relatively small amount of flooding. Ship designers usually calculate damage stability of a ship assuming static conditions with the requirements prescribed by the International Maritime Organization (IMO). Dynamic effects are much more pronounced during flooding, large and violent motions of the floodwater inside the unobstructed decks have an important effect on

* Corresponding author.
E-mail address: mohd.a.siddiqui@ntnu.no (M.A. Siddiqui).

https://doi.org/10.1016/j.apor.2020.102090
Received 12 December 2019; Received in revised form 30 January 2020; Accepted 12 February 2020

Nomenclature

ζ	wave elevation inside damaged compartment
ζ_a	wave elevation amplitude inside damaged compartment
η_i	motion response in incident waves, for sway $i = 2$, heave $i = 3$ and roll $i = 4$
η_{ia}	motion response amplitude in incident waves, for sway $i = 2$, heave $i = 3$ and roll $i = 4$
ω	angular frequency of regular waves generated by the wavemaker
ω^*	non-dimensional frequency of regular waves generated by the wavemaker
ω_{np}	natural frequency for piston mode resonance
ω_{np}'	natural frequency for piston mode resonance including effect of baffle
ω_{ns}	natural frequency for sloshing mode resonance
A	amplitude of incident regular waves
A_{44}	roll added mass about CoG
B	breadth of model
B_c	breadth of damaged compartment
B_{44}	linear roll damping coefficient
$B_{44,quad}$	quadratic roll damping coefficient
BM	height from center of buoyancy to metacenter
C_{44}	roll restoring coefficient
CoG	center of gravity
D	depth of model
d	length of side damage
GM	metacentric height in roll
g	acceleration due to gravity
h_c	height of damaged compartment
h_d	height of damage opening
I_{44}	roll moment of inertia about CoG
KG	height of center of gravity above keel
k	wavenumber
kA	wave steepness
L	length of model
L_c	length of damaged compartment
M	dry mass of model
M_b	solid ballast mass
M_w	floodwater mass
T	time period of regular wave generated by the wavemaker
T_d	draft of model

the ship motions and vice versa. Ruponen [2] mentions that usually after a damage event, flooding is divided in three phases:

1 Initial transient phase
2 Progressive flooding
3 Steady state behavior about a new equilibrium position.

Dynamic stability just after a damage event (Phase 1) is of greatest importance as the immediate behavior after the damage is critical for capsize occurrence. However, even after attaining a steady equilibrium condition (Phase 3), the dynamic behavior of a damaged ship in waves is considerably different from the intact condition. Study of the dynamic behavior can help in understanding critical conditions and thus improve design and safety requirements especially for passenger vessels.

Many numerical methods have been proposed to study the behavior of damaged ship sections. Spouge [3]was one of the first authors to study a damaged ship. He demonstrated the capsizing of the RO-RO vessel 'European Gateway' using a hydraulic orifice flow model and employed empirical equations to determine the center of gravity (CoG) of floodwater. Hydraulic orifice model is generally used for pressure-driven water flow between two regions connected with an opening. In their case, it was used for the flow between external environment and damaged ship compartment. Papanikolaou et al. [4], Spanos and Papanikolaou [5] and Jasionowski [6] simulated the coupled floodwater-ship motions using the lumped mass concept (floodwater is considered to be a rigid mass), whereas the floodwater free-surface is freely moving. Manderbecka et al. [7] also used a lumped mass method with a moving free surface and presented time-domain simulations of damaged ship motions with validation against experiments. More recently, fast simulation methods have also been employed, for example Acanfora and Cirillo [8] presented a method to examine the transient stage of flooding. They used a lumped mass method, considering the free surface of floodwater to be normal always to the modified gravity vector. Computational Fluid Dynamics (CFD) solvers have also become quite attractive to study damaged ship behavior due to increase in availability of computational resources. Gao and Vassalos [9] employed a commercial RANS solver to study forced roll motions of a damaged ship. They analyzed the damping effect of floodwater in a damaged ship as compared to intact condition. Gao et al. [10] used a hybrid method coupling a potential-flow solver for intact region and Navier-Stokes solver for the damaged region, to study the behavior of a damaged ship in waves. Sadat-Hosseini et al. [11] performed CFD simulations for a damaged passenger ship in calm water and in beam-sea waves. They compared results with experiments and demonstrated better agreement than potential-flow solvers but with significant computational cost. Hashimoto et al. [12] presented numerical simulations and experiments for forced roll motions and flooding test of a damaged Pure Car and Truck Carrier model. They also used a hybrid model as Gao et al. [10] combining a potential-flow solver with a Moving Particle Simulation. They presented good agreement between experiments and numerical simulations, showing that the simulation method reproduced ship's transient flooding well. Begovic et al. [13] presented CFD results for roll decay of intact and damaged ship models. They analyzed the effect of grid size and time step on numerical simulations and presented reasonable agreement with experimental data. The 23rd ITTC specialists committee on extreme motion and capsizing in waves, Papanikolau [14], conducted an international benchmark study where the accuracy of existing computational models was examined by comparing them against experimental motions of a damaged ship. There were five independent participants in this study. The benchmark study demonstrated disagreement among the results from the numerical simulations of the same ship. The presented models can predict well the behavior at non-resonant wave periods but have limitations in capturing roll resonance period and magnitude accurately depending on the simplifications used in the respective numerical technique, differences in roll viscous damping models, floodwater-handling method and wave-body interaction calculations. The 24th ITTC benchmark study, Papanikolau and Spanos [15], also presented a detailed analysis of the roll-decay data in intact and damaged conditions for a RO-RO ship model (PRR01), comparing experimental data with numerical studies by five participants. The benchmark data show that all numerical methods capture natural period and damping well for the intact condition. For the damaged scenario, all studies show deviations as compared to experimental values. The authors concluded that this can be due to modeling of the roll-damping terms and simplification in modeling of the floodwater-dynamics. It must be emphasized that both these important benchmark studies were performed almost 20 years ago. They provided significant insights in the understanding of damaged ship behavior and highlighted limitations on the numerical side. However, there has been significant development in numerical methods along the years. The increase in availability of computational power has rendered CFD as an important complementary tool in the study of damaged ships [9–13]. Nevertheless, full-scale time domain simulation is still complex

and extremely time-consuming. Therefore, due to the complex nature of the problem, detailed investigations need to be performed. They will help to assess the main parameters involved in the given problem. An experimental study may aid in understanding the complex interaction between ship motions and floodwater in a damaged compartment. Experimental data also serve as a database for validation of numerical codes for the scientific community.

Many authors have performed experimental studies on damaged ships in waves in model scale. Schindler [16] has provided a very detailed overview on damage stability requirements based on model tests (Stockholm Agreement) for RO-RO ships. Korkut et al. [17] conducted an experimental study on a 6-DoF damaged RO-RO ship model. They used a freely floating model in regular waves attached to the tank walls with slack moorings and no forward speed. They varied wave periods, wave headings and wave heights to demonstrate the effect of these parameters on a damaged ship and variation with respect to an intact ship condition. They noted that the damaged vessel response is highly dependent on wave frequencies, wave headings and natural frequencies of the model. Lee et al. [18] presented a theoretical and experimental study of a damaged Ro-Ro ship model experiencing flooding in regular and irregular waves. They examined three damage conditions and varied the wave height and heading, showing qualitative agreement between numerical and experimental data. Begovic et al. [19] conducted experimental studies on a frigate hull in intact and damaged conditions. Motion responses were calculated both in intact and damaged condition. Two geosim models, at 1:100 and 1:51 scale, were tested with zero forward speed in various wave headings and wave periods. The authors investigated nonlinear behavior and calculated Response Amplitude Operators (RAOs) for second harmonics, useful for validating nonlinear methods. Lee et al. [20] performed experiments to study 6-DoF motions for a damaged ship in regular beam-sea waves with aim to build a database for CFD validation. Khaddaj-Mallat et al. [21] performed experiments on a damaged ship model and identified damage opening area, damage location and air compressibility in a damaged compartment as important parameters for investigating flooding in damaged ships. Manderbecka et al. [22] conducted experiments on a box-shaped barge with damage on the side. They demonstrated the effect of compartment width and layout on transient flooding. Effect of initial stability on the flooding process was also examined. The authors noted that a damage event usually leads to increase in damping and natural period for roll motion. Domeh et al. [23] conducted experiments on a damaged ship model, examining the effect of compartment permeability and damage orifice size on the model behavior in waves. They also studied the effect of forward speed on the motion responses of a damaged ship model. Acanfora and De Luca [24] performed experiments on a damaged ferry hull in beam-sea waves and investigated the effect of damage location on ship motions. They also investigated the effect of compartment damage on roll period and damping. Acanfora and De Luca [25] extended the work in [24] by using a realistic modeling for the damaged compartment. They also performed experiments assuming a damaged engine compartment and focusing on the effects of deck and obstructions for the roll motion in beam-sea waves. Cichowiz et al. [26] presented experiments on a cylindrical body in forced roll motion with an open-to-sea compartment. They highlighted the importance of understanding roll damping behavior for ships in damaged condition. Palazzi and de Kat [27] performed experiments on a damaged ship model with focus on the effect of air compressibility in airtight damaged compartment. Ruponen et al. [28] studied air compressibility effects on motions of a damaged ship using a full-scale model to avoid scaling issues associated with air compressibility. They noted that air compressions can slow initial flooding largely. Bennett and Phillips [29] studied experimentally the effect of floodwater on the ship motions and wave loads. They also presented transient flooding test results demonstrating the effect of sudden damage on ship motions. More recently, Gu et al. [30]presented experiments on a combatant vessel and analyzed the effect of floodwater on its stability. They also discussed damaged ship motion RAOs and wave-induced loads on the damaged ship model from the experiments.

Many of the aforementioned experimental studies focus on the transient flooding cases, survivability in damaged conditions and time to flood measurements. Some studies discuss free roll decay tests and effect of various parameters on roll damping behavior of a damaged ship. Studies like Korkut et al. [17], Begovic et al. [19], Acanfora and de Luca [24,25], and Gu et al. [30] focus on the dynamic behavior of a freely-floating stationary damaged ship in waves at its equilibrium position after flooding has taken place. In fact, though the most important phase is the initial transient flooding, it is also important to study the behavior of a floating damaged ship in waves. The former usually governs whether or not capsizing takes place, the latter will help in decision implementation on evacuation or in guiding the ship safely to the nearest port.

The floodwater in a damaged compartment of a ship can experience resonance behavior. Sloshing and piston mode resonance can be of particular significance. Sloshing is an internal flow problem associated with resonance of a liquid in a closed tank. Faltinsen and Timokha [31] studied sloshing in a tank with various structures and configurations. Piston mode resonance is a coupled external/internal flow problem associated with an opening and appears as a pumping in-and-out flow. It has been studied extensively for harbor resonance (Miles and Munk [32]) and moonpools (Molin [33], Faltinsen et al. [34]). Kristiansen and Faltinsen [35] analyzed experimentally and numerically the effect of piston mode resonance on ship motions when the ship section is close to a terminal wall and resonance occurs in the gap between them and reported important effects near resonance. Fredriksen et al. [36] studied wave response of a 2D body with moonpools using experiments and numerical schemes. They concluded that the piston mode frequency strongly affects the heave motions. Kong and Faltinsen [37] numerically analyzed the effect of sloshing and piston mode resonance in a damaged ship by a linear potential flow method. They demonstrated good agreement with ITTC benchmark experiments, capturing the peaks in roll motions quite well. de Kat [38] studied numerically and experimentally the motions of a ship with a partially filled tank and presented the effect of filling ratios on first natural mode of sloshing in a flooded compartment. [25] also demonstrated sloshing modes for a damage case without an opening in their Fig. 20 and observed excitation of the second sloshing mode due to influence of the engine layout. To our knowledge, no experimental studies available in literature focus specifically on sloshing and piston mode resonance frequencies for a damaged ship and their effect on damaged ship motions in waves. Excitation of resonance can be critical in some cases for the motions as shown in some mentioned experimental studies and also demonstrated in our work. Resonance behavior in the damaged compartment can also lead to important global and local loads. Begovic et al. [39] analyzed the impact of damage conditions on the vertical and horizontal shear force and bending moment for a naval ship model and reported that the shear force/bending moment behavior can be quite different as compared to an intact ship. Gu et al. [30] also demonstrated the impact of damage on hull girder loads. Both studies analyzed global loads but resonant behavior in the damage compartment can also cause local loads like roof impact, hydraulic jump like condition (shown for forced heave motion in [1]) etc. without necessarily causing large ship motions. Kong and Faltinsen [37] also showed very large free surface amplitude near first natural piston mode frequency causing large dynamic pressures on the deck, which may lead to local structural failures.

In the present work, we examine the behavior of a damaged ship section in waves with focus on the effect of sloshing and piston mode resonance, taking the numerical work by Kong and Faltinsen [37] as inspiration and extending in more detail the sloshing studies performed by de Kat [38], Acanfora and de Luca [24,25]. This work also serves as a continuation to the forced heave motion tests of a damaged section by Siddiqui et al. [1]. We study both an intact and damaged (same section with damage opening on the side) freely floating model in regular

beam-sea waves. This is done because beam-sea waves cause major roll response, if we exclude parametric-roll occurrence. The damage is modeled as a side damage in the midship region, rectangularly shaped, and with longitudinal dimension large compared with the ship cross-section dimensions. In this way, the problem may be idealized as two-dimensional (2D) in the cross-sectional plane. Free-roll decay tests are carried out to estimate the natural roll period in intact and damaged conditions. Detailed analysis is performed to understand the effect of floodwater on roll damping of a damaged ship section. The experiments in waves analyze a wide range of frequencies including the natural sloshing and piston mode resonance frequencies for the damaged flooded compartment. The influence of sloshing and piston mode resonance on body motions in waves is examined for two initial loading conditions. Air compressibility effects inside the damaged compartment are examined for the freely-floating body in waves. The effect of damaged-compartment and damage-opening sizes are also studied. Finally, transient flooding cases have been examined where the model experiences sudden abrupt flooding. Bennett and Phillips [29] and Manderbecka et al. [22] have performed transient flooding tests and showed the effect of abrupt flooding on ship motions. Both of the aforementioned studies use a mechanism where damage openings are initially sealed and can be opened suddenly to simulate transient flooding. In our case, we have a larger opening and due to restrictions in the wave flume, we could not simulate such a mechanism. Instead, we studied the scenario where the model is initially dry, and flooding takes place due to the ship motions. Soon after the model opening gets exposed to external water, flooding occurs. This was likely the case with Estonia (1994); it seems that the bow visor door did not close properly and due to slamming loads the bow visor door was damaged. Therefore, seawater accumulated on the car deck leading to capsize and tragic loss of 852 lives. The effects of wave period, wave steepness and initial stability are studied for transient flooding cases.

The remaining of the paper is structured as follows. Section 2 describes the experimental setup and conditions used in the physical analysis. It gives a detailed description of the model section used and layout of the equipment and wave probes inside the model and in the tank flume. Section 3 describes the natural resonance frequencies for the damaged compartment. Details of the calculations for the resonance frequencies can be found in Siddiqui et al. [1]. Section 4 presents measurements and error analysis performed on the data acquired from various devices during the experiments. Sources, which may lead to error in measurements, are also listed. Section 5 presents in brief a strip theory method to analyze the current damage scenario. It is aimed to provide a cross-check of, and to complement, the experimental data. Section 6 presents the results and provides a physical analysis based on them. For the damaged section in regular waves, linear RAOs are presented for sway, roll and heave along with wave elevation RAOs inside the damaged compartment. In case of transient flooding, time series for the wave elevation inside the compartment are shown. The measurements are complemented by side-view images from video recordings of the tests. Finally, conclusions and challenges identified in the present study are provided to benefit readers with future work.

2. Experimental set-up and test conditions

A detailed setup of the wave flume and of the model is described in [1]. In brief, the wave flume is 15 m long, 0.58 m wide, has a water depth of 0.95 m and is located at the Marine Technology center, Trondheim, Norway. The model encompasses the width of the flume and is slightly smaller than the flume width to obtain predominantly 2D behavior. The wave flume has plexiglass walls, which allow a clear visualization of the free surface interactions with the body. It is equipped with a piston wave maker on one side and with a parabolic beach for transmitted-wave absorption at the opposite end.

2.1. The model

The model is designed as part of a midship section and location of the damage is chosen to be at the side. The large clean deck can be assumed as a simplified midship section of a RO-RO ship model. The model was made of aluminum plates (bottom and side plates), divinicell (ballast region in the bottom), i.e. compressed foam, wood (overall structure) and fiberglass on the front side for visualizing the floodwater. Prior to starting the experiments, the roll moment of inertia about the x-axis (CoG) and CoG of the intact model were determined using swing tests in air. A schematic view of the designed and actual models with Cartesian coordinate system Oxyz and origin at the center of gravity with ballast mass is defined in Fig. 1. Main dimensions of the model and of the internal compartment are described in table 1. Hydrostatic parameters for the model in intact and corresponding damaged condition are provided in table 2. The lost buoyancy method, as described by Biran and Pulido [40] is used to calculate the parameters for the damaged section.

2.2. Equipment and test description

A semiautomatic digital camera with a video capturing rate of 60 fps was used. The frame quality varied for some videos, but it was always at least 640 × 480 pixels. Two twin wire wave probes were located inside the body at a distance 0.25B (WP1) and 0.75B (WP2) from the opening to measure the wave elevation inside the damaged compartment. Two wave probes were placed outside the compartment, respectively, 5 m downstream from the wave maker/3 m upstream from the body (WP3) and 3 m upstream from the beach/4 m downstream from the body (WP4) to measure wave elevations in the wave flume. Three accelerometers (Acc 1–3) were placed on the model to verify the heave and roll measurements computed from the video data. Fig. 2 shows a top view of the model with location of wave probes and

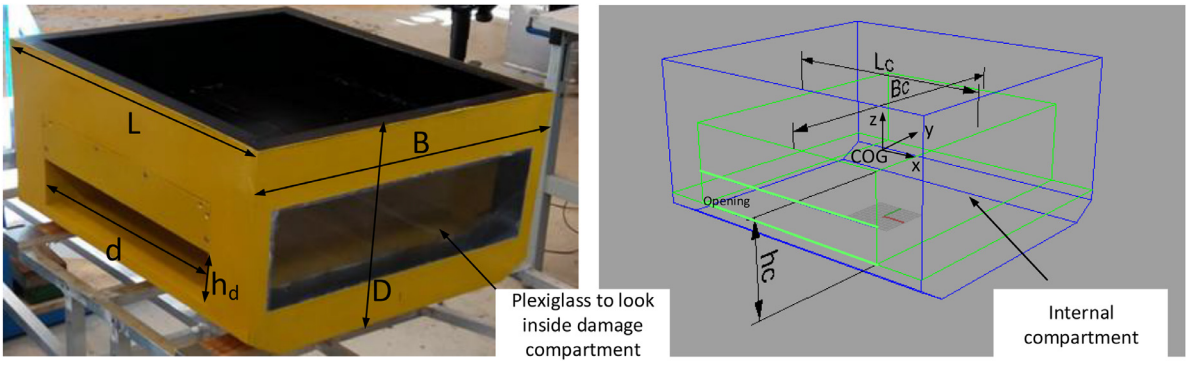

Fig. 1. Definition of geometric variables in the three-dimensional view of the actual cross-section model (left) and definition of geometric variables for the internal compartment (right) (figure from [1]). Dimensions of geometric variables are provided in table 1.

Table 1
Dimensions of the section model and compartment.

Length along tank width (L)	0.57 m
Breadth (B)	0.5 m
Depth of model (D)	0.3 m
Side damage length (d)	0.4 m
Side damage height (h_d)	0.08 m
Length of compartment (L_c)	0.4 m
Breadth of compartment (B_c)	0.5 m
Height of compartment (h_c)	0.15 m
Intended Scale	1:40

accelerometers. Sampling frequency for all data recorded in the measurements was 200 Hz. The duration of each test varied between 120 and 180 s depending on the wave period T, so to have at least 60T duration in each test. However, when wave reflection from the wavemaker was evident, the analyzed time series was truncated. Regular waves are generated using a flap wavemaker hinged 5 cm above the flume bottom with a dry backside. It has a linear ramp up during the first few seconds and similar ramp down during the end of input signal. The model was positioned in the flume as shown in Fig. 3. Two wave steepnesses were used and wave periods were selected within $T = 0.6$ s - 2.7 s (at a model scale). The oscillation periods for incident regular waves were selected to give full-scale oscillation periods in the range of 4 to 18 s with a scale of 1:40. These are realistic incident wave periods encountered by sea-going ships. The spacing between time periods is not uniform but selected so as to capture resonance phenomena in adequate detail. The waiting time in between the tests was 5–10 min depending on the incident wave period, to allow the flume water to attain a calm condition.

The centerplane of the model is at a distance of 8 m from the wavemaker. The damaged opening faces the wavemaker side, thus the model is in a beam-sea wave scenario. Two slack horizontal moorings were also used to control drift in sway direction. They have minor effect on the natural roll or heave periods. This setup also helps to restrict yaw motion and therefore the model has three degrees of freedom in sway, heave and roll. The test conditions in regular waves are summarized in table 3. In this scenario of the damaged ship section in waves, the model is initially in a stable condition after being flooded and having attained equilibrium. The damage-compartment size is halved by placing a watertight plate at the centerplane. This is referred to as half compartment damage and helps in analyzing the effect of asymmetrical flooding. The freely-floating model in intact and damaged conditions was examined at selected loading conditions. Drafts at the two examined loading conditions for an intact section and corresponding drafts in damaged conditions are provided in table 4. Effect of change in size of the damage opening is also examined. The opening sizes and corresponding names used in this text are provided in table 5. Effect of an airtight compartment is examined for the damaged condition. In this case, all openings above the floodwater level inside the damaged compartment are sealed. Moreover, as a special case, the transient stage of flooding is investigated. This is the most crucial phase in flooding and capsize usually takes place during this phase. In order for capsize to not occur in the model tests and to not complicate the test program, it is important to study some simplified cases of transient flooding. In our case, the model is initially freely floating and dry and the damage opening edge lies above the waterline. As waves excite roll motions, sudden and abrupt flooding takes place leading to large transient motions. In the scenario of transient flooding, half compartment damage is used, since it will lead to larger roll motions with smaller amount of floodwater.

3. Natural frequencies for floodwater inside the damaged compartment

Sloshing and piston mode resonance may be excited inside the damaged compartment. Sloshing mode refers to a mode shape similar as if the compartment was closed. Piston mode resonance is similar as in a harbor corresponding to close to a wave node with maximum/minimum horizontal water velocity at the opening. The inflow/outflow occurring through the damage opening can be assumed to behave as a wavemaker for the internal floodwater. It is also excited directly by roll and sway motions. For a 2D rectangular tank with water depth h and breadth B_c, the natural frequency of sloshing mode j is given by

$$\omega_{nsj} = \sqrt{g\frac{\pi j}{B_c}\tanh\left(\frac{\pi j}{B_c}h\right)}$$

Table 6 shows the non-dimensional sloshing frequencies for the first, second and third 2D sloshing modes, i.e. $j = 1$, 2 and 3, for a fully damaged compartment. In our case, we consider sloshing along the compartment breadth as the dominant sloshing direction. We also study cases where the model has half-compartment damage and an initial heel angle. For this case, we need to study sloshing in an inclined closed tank with respect to the vertical direction. This is described in section 4.6.1 of Faltinsen and Timokha [31]. Fig. 4 defines the relevant parameters related to a damaged floating body with an initial heel angle. Table 7 shows the non-dimensional sloshing frequencies for the first and second sloshing modes, i.e. $j = 1$ and 2, for half compartment. Figure 4.17 in Faltinsen and Timokha [31] describes the effect of inclination on natural sloshing frequencies in a tank using the ratios $(h-h_2)/h$ and h/l. The values of these parameters in our cases are summarized in table 7. From them, we conclude that the effect of inclination on first natural sloshing frequency is quite small, in fact it is 98% of the natural frequency for a vertical tank with the same dimensions.

There are also piston (pumping) mode resonance frequencies associated with in/outflow through the opening. The detailed analysis for calculation of piston mode frequencies with 2D flow is provided in Siddiqui et al. [1]. Table 8 shows the non-dimensional piston mode frequencies for the first, second and third piston modes, i.e. $j = 1$, 2 and 3, for a fully damaged compartment. Using a similar argument as that for sloshing in a half-compartment damage case, we can neglect the effect of inclination on the natural frequencies. The effect of the upper opening edge (baffle) on the modeshapes is discussed to in detail in [1]. Table 9 shows the non-dimensional piston mode frequencies for the first and second piston modes, i.e. $j = 1$, 2, for half compartment. However, we cannot out rule the effect of 3D sloshing and piston mode resonances, which were observed in a few cases at high frequency.

Table 2
Hydrostatic parameters of the model in intact condition and damaged condition for a particular draft.

	Intact Condition		Damaged Condition	
Draft (T_d)	7 cm	8.5 cm	11 cm	15.5 cm
Dry mass (M)	14.5 kg	14.5 kg	14.5 kg	14.5 kg
Solid Ballast mass (M_B)	4 kg	8 kg	4 kg	8 kg
Center of gravity from Keel (KG)	0.105 m	0.125 m	0.095 m	0.115 m
Roll moment of inertia of model about x-axis with ballast mass (I_{44})	0.545 kg m^2	0.545 kg m^2	0.545 kg m^2	0.545 kg m^2
Transverse metacentric height (GM)	0.175 m	0.2 m	0.048 m	0.03 m
Static Floodwater mass (M_w)	–	–	12 kg	21 kg

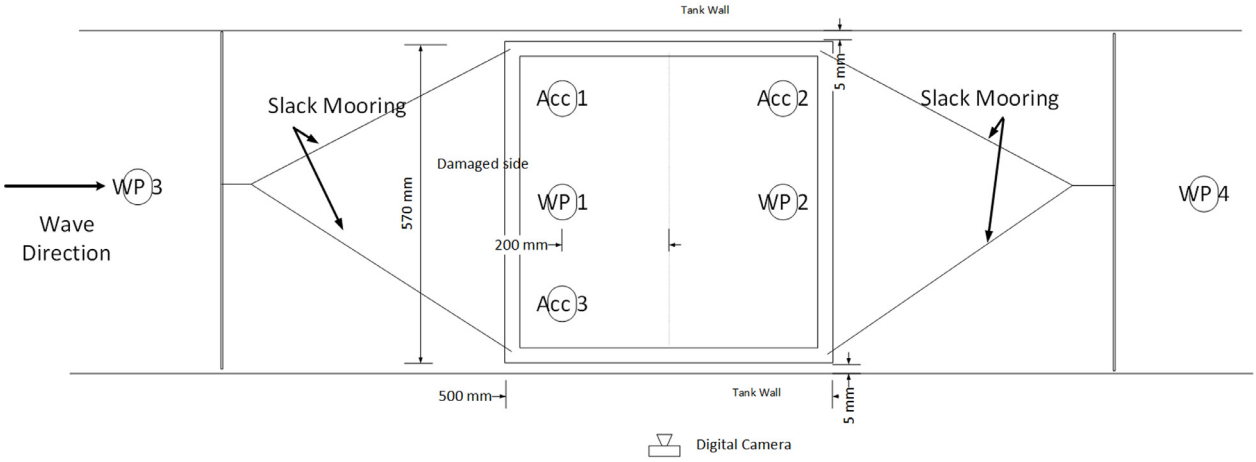

Fig. 2. Sketch of the damaged section (top view) with location of wave probes and accelerometers.

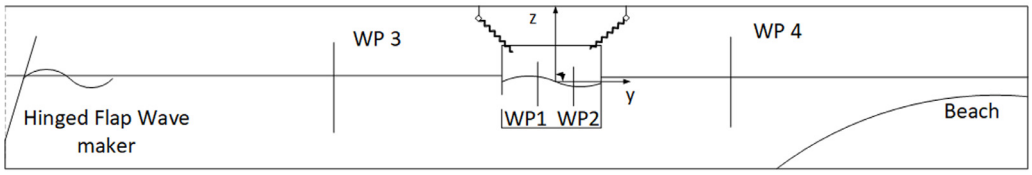

Fig. 3. Sketch (not to scale) of the experimental setup in the wave flume for tests in regular waves with the location of model and wave probes.

4. Data and error analysis

Time histories of wave probe signals contain raw data at the input frequency as well as some high-frequency content. The raw signals from the instruments were band-pass filtered to remove frequencies above 10 Hz and below 0.5 Hz (slow drift component). This removes all high-frequency content, above the third natural sloshing frequency, and low-frequency effects like seiching in the flume. The wave amplitudes of the wave probes inside and outside the compartment are measured by performing Fast Fourier Transform (FFT) analysis of the time series data. The motions of the model were calculated through the analysis of the video recordings from the tests. Two markers were placed at known locations (one port and one starboard side) on the front plexiglass side plate (yz plane) of the model facing the camera and then processed to get a time series for sway, heave and roll motions using image-processing toolbox in MATLAB. For each incident wave period T, the sway, heave and roll motion amplitudes are calculated from their time series as the mean of motion peaks for 5–10T in the steady-state region and considering that no effect of reflection from the wavemaker is present. The steady-state motion values are extracted at the main incident wave frequency component by excluding any drift/higher order harmonic motion. For heave and roll motions, negligible drift is observed for all cases and frequencies. Since the moorings remain slack in most cases, the model is free to drift in sway within a certain range. To avoid any effect of pure drift motion on sway RAOs, the sway motions in the steady-state region are filtered, excluding any drift motions (similarly as shown in Fig. 10 of Acanfora and de Luca [24]).

4.1. Error sources

Main error sources in the model tests are:

- Meniscus effect caused by surface tension in the steel wire wave probes. Faltinsen and Timokha [31] mention a bias error less than the diameter of the steel wire. For small motions of the model at smaller wave steepness, the wave elevation may be too small and thus cause a larger relative error.
- Three-dimensional behavior is present and observed mainly near natural resonance frequencies in roll and heave for the model, where the motions can be large. For the damaged model, 3D flow effects occur due to discontinuity in cross-sectional shape at the ends of the damaged compartment as well at the longitudinal ends of the damage opening. These 3D effects can cause the model to strike the flume glass walls, rarely resulting in spikes in the measurements. These spikes are removed while filtering.
- There are also small viscous shear effects involved due to the water between the model and flume glass walls. However, these forces are generally negligible compared to wave-induced pressure forces on the model.
- Reflection from the flap wave maker is a potential error source and hard to prevent because the installed automatic absorption system did not work properly. However, data with clear evidence of wave maker reflection were disregarded. The wave absorption by the beach can be less effective for longer incident wave periods ($T >$ 1.5 s) and larger values of the wave steepness, as mentioned by Kristiansen [41].

Table 3
Test matrix for model in waves.

Type	Wave period (s)	Wave steepness (kA)	Condition	Compartment damage	Repetitions
Freely floating in waves	0.5 – 2.2	0.033	Intact	–	–
Freely floating in waves at two drafts	0.5 - 2.5	0.033,0.066	Damaged	Full, half	5
Freely floating in waves without ventilation	0.5 – 2.5	0.033	Damaged	Full	–
Freely floating in waves with change in opening size	0.5 – 2.5	0.033	Damaged	Full, half	–
Transient flooding	0.5 - 1.5	0.033,0.066,0.1	Damaged	Half	2–3

Table 4
Drafts for same loading conditions in intact, full and half compartment damage conditions.

Intact Draft	Corresponding draft for full compartment damage	Corresponding draft for half compartment damage towards the damaged side
7 cm	11 cm	12.5 cm
8.5 cm	15.5 cm	16.5 cm

Table 5
Damage openings used in the experiments.

Openings	Width of opening d (m)	Height of opening h_d (m)
Opening 1 (O1)	0.4	0.08
Opening 2 (O2)	0.3	0.08
Opening 3 (O3)	0.2	0.08

Table 6
Relevant non-dimensional sloshing resonance frequencies ω_{nsj} for the examined full damaged compartment at two drafts by assuming closed compartment. (h is water depth).

Draft	h (m)	$\omega_{ns1}\sqrt{\frac{B}{2g}}$	$\omega_{ns2}\sqrt{\frac{B}{2g}}$	$\omega_{ns3}\sqrt{\frac{B}{2g}}$
11 cm	0.06	0.78	1.45	1.99
15.5 cm	0.105	0.95	1.65	2.13

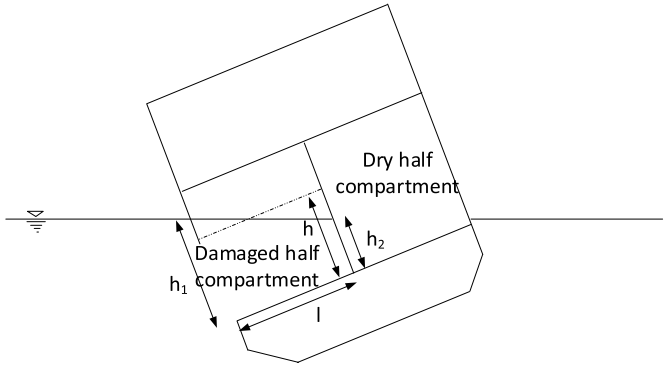

Fig. 4. Asymmetric floating position due to half compartment damage.

Table 7
Relevant non-dimensional sloshing resonance frequencies ω_{nsj} for the examined half compartment damage at two drafts. See Fig. 4 for definition of h_1, h_2, h and l.

Draft	h_1 (m)	h_2 (m)	h (m)	h/l	(h- h_2)/h	$\omega_{ns1}\sqrt{\frac{B}{2g}}$	$\omega_{ns2}\sqrt{\frac{B}{2g}}$
12.5 cm	0.075	0.05	0.0626	0.25	0.2	1.43	2.39
16.5 cm	0.115	0.0782	0.0966	0.386	0.19	1.62	2.48

- The effect of slack mooring on the model is a possible error source. This is usually observed for certain wave periods when the slow drift is large, possibly causing jerk forces on the model. In order to limit this error source, we examined the steady-state regime within 5–10 wave periods and checked for jerk-like motions. The part of the time history without such motions only has been included in the analysis.
- Bias error in the calibration of measuring instruments, and also parallax error in videos due to the glass wall, can cause some small errors.

Table 9
Relevant non-dimensional piston mode frequencies ω_{npj} and ω_{npj}' (effect of baffle) for the examined half compartment damage at two drafts.

Draft	h (m)	$\omega_{np1}\sqrt{\frac{B}{2g}}$	$\omega_{np1}'\sqrt{\frac{B}{2g}}$	$\omega_{np2}\sqrt{\frac{B}{2g}}$	$\omega_{np2}'\sqrt{\frac{B}{2g}}$
12.5 cm	0.0626	0.59	0.59	2.06	2.06
16.5 cm	0.0966	0.65	0.64	2.215	2.2

4.2. Uncertainty analysis and repeatability

Specific regular wave conditions were repeated up to five times to assess test repeatability. Mean value of a certain variable is estimated as $\bar{x} = \frac{\sum_5 x_i}{5}$, where x_i is the measurement for i^{th} repetition. Absolute deviation of the variable of interest from its mean value is estimated as $\Delta\bar{x} = \frac{\sum_5 |x_i - \bar{x}|}{5}$ and from them we can measure relative absolute deviation as $\frac{\Delta\bar{x}}{\bar{x}}\cdot 100\%$. The repeatability of the experiments and related errors are discussed in section 6.

5. Complementary numerical analysis

Assuming negligible 3D effects during the tests, a linearized strip-theory numerical method was implemented for calculating intact and damaged ship section motions, incorporating a nonlinear roll viscous damping term based on numerical calculations for the damaged scenario. Consistently with strip theory [42,43] the body is divided into strips along its elongation direction. In each strip, the loads are found as 2D in the cross-section plane and multiplied by the strip length to obtain corresponding 3D-load contributions. Summing the contributions from all strips provides the total 3D loads acting on the body. In our case, for the intact ship section we need to solve only one 2D seakeeping problem and then multiply the 2D loads by L. For the damaged ship section, the 3D ship model has intact and damaged strips and the seakeeping problems are solved for both the damaged and intact strips and multiplied with respective section lengths to get the total 3D loads (Fig. 5). Consistently with linear theory, the 2D cross-section loads are found by splitting the seakeeping problem in radiation and diffraction problems. Their solutions provide, respectively, the added-mass, damping and restoring coefficients, and the wave excitation loads. Generally, for strip-theory seakeeping methods, potential flow solvers with additional nonlinear roll viscous damping terms are employed to solve these problems. We instead use the open-source viscous CFD solver OpenFOAM with laminar flow assumption. An error source is that the free vorticity flow is likely to be turbulent. Since flow separation occurs from sharp corners, the boundary layer plays a secondary role. Both intact condition and full compartment damage were considered. The latter assumes that the damaged compartment is fully ventilated. The total loads are estimated from the steady-state solution of the radiation and diffraction problems and then extracting the wave-

Table 8
Relevant non-dimensional piston mode frequencies ω_{npj} and ω_{npj}' (effect of baffle) for the examined full compartment damage at two drafts.

Draft	h (m)	$\omega_{np1}\sqrt{\frac{B}{2g}}$	$\omega_{np1}'\sqrt{\frac{B}{2g}}$	$\omega_{np2}\sqrt{\frac{B}{2g}}$	$\omega_{np2}'\sqrt{\frac{B}{2g}}$	$\omega_{np3}\sqrt{\frac{B}{2g}}$	$\omega_{np3}'\sqrt{\frac{B}{2g}}$
11 cm	0.06	0.3	0.3	1.02	1.02	1.68	1.68
15.5 cm	0.105	0.364	0.359	1.257	1.24	1.953	1.92

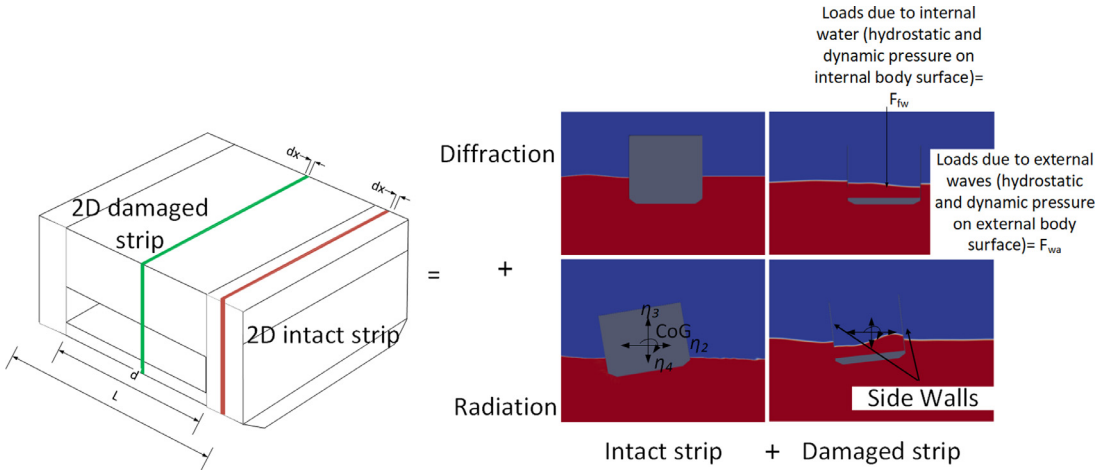

Fig. 5. Strip theory illustration for a damaged section (decomposition into radiation and diffraction problems).

frequency contribution.

OpenFOAM implies a nonlinear method with nonlinear free surface conditions that accounts for the floodwater inside the compartment for damaged conditions (radiation/diffraction loads are calculated using pressure integration along the internal and external wetted parts of the damaged ship section). The no-penetration body boundary condition is applied at the instantaneous position of the body surface for the radiation problem and mean body position of the body surface for the diffraction problem. Since, the radiation problem solves for the pressure on the instantaneous body surface, the added mass terms contain the dynamic effect of the hydrostatic pressureThe radiation moments are evaluated about the CoG. The volume of fluid (VOF) method is used in OpenFOAM for capturing the free surface, which can be diffusive. We try to minimize this by using a fine spatial mesh near the free surface and a second order Crank-Nicholson scheme in time. The radiation problem is amplitude dependent and we use two amplitudes, 8° and 14° for forced roll motion and 0.005 m and 0.01 m for forced sway and heave motions of CoG, to check for nonlinear behavior. Nonlinear mean and higher harmonic force amplitudes are small and are, in general, neglected. However, nonlinear viscous damping must be included especially for roll motions at resonance. This cannot be properly handled within the described linearized seakeeping approach and is included for the damaged section as an additional quadratic damping term based on OpenFOAM forced roll calculations and is discussed later. The diffraction problem is solved considering the same setup as in the experiments with the body fixed at the initial floating location of the body. The diffraction forces at any incident wave period are calculated by taking the mean of the steady-state values over 3–5 time periods (depending on the incident wave period).

We assume complex time dependence exp($i\omega t$), where i is the complex unit and ω is the circular incident wave frequency. We define η_2, η_3 as the sway and heave motion of the CoG. Furthermore, η_4 is the angular roll motion. The wave excitation moment is taken about the x axis through CoG. The linear equations of motion in the frequency domain can be expressed as

$$\left\{-\omega^2\begin{bmatrix} A_{22}+M+M_b & A_{23} & A_{24} \\ A_{32} & A_{33}+M+M_b & A_{34} \\ A_{42} & A_{43} & I_{44}+A_{44} \end{bmatrix} + i\omega\begin{bmatrix} B_{22} & B_{23} & B_{24} \\ B_{32} & B_{33} & B_{34} \\ B_{42} & B_{43} & B_{44} \end{bmatrix} + \begin{bmatrix} 0 & 0 & 0 \\ 0 & C_{33} & 0 \\ 0 & 0 & C_{44} \end{bmatrix}\right\}\begin{bmatrix} \eta_2 \\ \eta_3 \\ \eta_4 \end{bmatrix} = \begin{bmatrix} F_2 \\ F_3 \\ F_4 \end{bmatrix} e^{i\omega t} \quad (1)$$

Here, A_{jk}, B_{jk}, C_{jk}, (j,k = 2,3,4) are the added mass, damping and restoring terms, F_k exp(iωt), is the wave excitation force/moment in sway (2), heave (3) and roll (4), respectively, M is the dry mass of model and M_b is the solid ballast mass. Heave is uncoupled from sway and roll only in the intact numerical case. The added mass and restoring coefficients are, in general, not unique. The unique term is $-\omega^2 A_{jk} + C_{jk}$, which is obtained by the described numerical method. We have chosen to estimate C_{jk} by a quasi-steady hydrostatic analysis as it is done for intact ships. The 2D restoring coefficients in heave and roll for an intact cross-section (i.e. with unit length perpendicularly to the cross-section) are $c_{33} = \rho g B$ and $c_{44} = \rho g \nabla GM$, where ρ is the mass density of water, ∇ is the displaced cross-sectional area and GM is the metacentric height for the cross-section. For the damaged section, we consider the quasi-steady hydrostatic effect of the floodwater in the compartment. For a fully ventilated damaged cross-section (i.e. with unit length perpendicularly to the cross-section), restoring effects could only come from the side walls of the compartment (indicated in the bottom-right panel of Fig. 5). However, their thickness is only 2.5 mm so we assume that their restoring effect can be neglected, therefore, $c_{33} = 0$, $c_{44} = 0$, in this case. The sectional added mass and damping coefficients are obtained from the time series following the approach in Vugts [44]. We will in later discussion, demonstrate calculations with a viscous drag term $B_{44,quad}\dot{\eta}_4|\dot{\eta}_4|$ in the roll equation.

6. Results and discussion

In this section, we examine freely-floating section in regular waves. Results from roll decay tests for the intact and damaged sections and transient flooding in regular waves for a damaged model section are also presented. Hereafter, the term linear is used to indicate the contributions to the examined variables, extracted from the analysis, that are associated with the incident-wave frequency. The results are documented in terms of linear wave elevation RAOs inside the damaged compartment and linear motion RAOs (sway, heave and roll) for the freely-floating section. To assess the influence of damage and resulting floodwater on the body motions, both intact and damaged conditions were examined. A thin wooden plate was placed over the damaged opening and sealed watertight. Intact tests were performed for one wave steepness i.e. kA = 0.033. For the damaged section, two wave steepnesses i.e. kA = 0.033 and 0.066 have been examined. These values seem to be small but at higher steepness we observe 3D behavior with yaw motions causing contact of model section with tank walls. Since 2D behavior is the focus of this work, we avoid higher kA values. Also, higher values of the wave steepness may cause capsizing. We must note that for the damaged condition, the coupled floodwater-body motion can introduce non-negligible nonlinearities. On the other hand, the focus of the present work is to analyze effect of sloshing and piston mode resonance on the linear response of a damaged ship. Therefore, based also on the work in Begovic et al. [19], we present the results in

terms of linear RAOs (first-order harmonic) as they help in the understanding physical behavior relevant in this case. Discussion is presented for RAOs with respect to resonance behavior of floodwater inside the damaged compartment. Sloshing and piston-mode resonance scenarios are presented using images from the tests with the green bold lines representing the 2D internal wave inside the compartment. All results have been made non-dimensional as follows:

$\omega^* = \omega\sqrt{\frac{B}{2g}}$, $\zeta^* = \frac{\zeta_a}{A}$, $\eta_i^* = \frac{\eta_{ia}}{A}$, $i = 2$ for sway and $i = 3$ for heave, $\eta_4^* = \frac{\eta_{4a}}{kA}$. Here η_{ia} and ζ_a denote the motion amplitude and wave elevation amplitude inside the damaged compartment, respectively and A is the incident wave amplitude.

6.1. Free-roll decay tests

Free-roll decay tests are performed to determine the natural roll period and roll damping of the model both in intact and damaged conditions. The tests are performed in still water. Coupling effects with the other degrees of freedom are neglected and the roll motion is assumed to be of the form

$$(I_{44} + A_{44})\ddot{\eta}_4 + B_{44}\dot{\eta}_4 + B_{44,quad}\dot{\eta}_4|\dot{\eta}_4| + C_{44}\eta_4 = 0 \quad (2)$$

where I_{44} is the moment of inertia in roll about the x-axis through CoG, A_{44} is the added moment of inertia in roll, B_{44} is the linear damping coefficient, $B_{44,\ quad}$ is the quadratic damping coefficient, C_{44} is the linear restoring coefficient and η_4 is the roll motion. CFD calculations were not done for the free decay tests. Instead the added mass A_{44} is estimated using $A_{44} = (\frac{2\pi}{T_{n4}})^2 C_{44} - I_{44}$, where T_{n4} is the natural roll period, which is calculated as the mean of the first three oscillation periods in the experiments. Furthermore, I_{44} is defined in Section 2 and C_{44} is calculated as defined above. An optimization technique is used to find the best fit for the experimental data and therefore calculate the linear and quadratic damping coefficients. Runge-Kutta 4th order scheme is used to solve for the roll angle in eq. (2). The results from this strategy will be indicated as 'fitted data' in the comparison against experimentally measured free-roll decay data.

The roll natural periods and linear and quadratic damping coefficients determined from the experiments for the examined cases are documented in table 10. Model tests for free-roll decay of a RO-RO ship model in intact and damaged condition (described in benchmark studies [14,15]) demonstrated that the natural roll period and roll damping increase going from intact to damaged condition for examined loading conditions (KGs). Other works, e.g. [19,22–25,30] have supported this finding. This behavior is confirmed by numerical studies from different participants in [14,15] although with deviations as compared to the experiments. Kong and Faltinsen [37] also confirmed numerically that the natural periods for roll and heave increase in damaged condition with internal flooding. We observe similar behavior in present experiments. We notice a large change in the natural roll period from intact to damaged condition. An important reason is the decrease of C_{44}. The damping is also considerably larger because of the inflow/outflow of the floodwater. Linear damping mainly consists of wave radiation damping, whereas quadratic damping is associated with viscous and vortex shedding effects. The absolute value of linear damping increases from an intact section to a damaged section. If we consider the non-dimensional values, to avoid the effect of increased draft in damaged condition, we observe that the non-dimensional linear damping decreases slightly. The linear damping has similar values for all three damage opening sizes. It increases very slightly for the smaller openings. The quadratic damping is not large for the intact section because there are no appendages or bilge keels. The quadratic damping for the damaged section is believed to be mainly associated with the vortex shedding at the opening and its effect on the local pressure distribution. The strength of the shed vorticity depends on the magnitude of the inflow/outflow velocity through the opening as well as on the geometric details. Generally speaking, the damping for given inflow/outflow increases with decreasing interior angle at the separation point. The magnitude of inflow/outflow velocity depends on the opening area because of continuity of water mass. A dominant effect of the air cushion in the airtight condition is to restrict changes in water mass in the compartment and therefore restricting the inflow/outflow through the opening (piston mode behavior). Table 10 shows that the dimensional quadratic damping is largest for the damage Opening 1 (largest opening) with ventilated compartment. If we consider non-dimensional values of the quadratic damping with respect to the damaged opening area, the order is reversed with Opening 3 (smallest opening) having the largest quadratic damping coefficient. The quadratic damping decreases significantly for a damaged compartment in airtight condition as compared to the ventilated case. This suggests that the inflow/outflow is highly reduced, leading to smaller vortex shedding at the opening and, therefore, much smaller quadratic damping.

Figs. 6-8 show a reasonable agreement between the measured and fitted roll time histories for the intact and damaged sections. The predicted curves for a damaged section have higher deviation as compared to an intact section but the overall data fit seem to be in reasonable agreement with the physical decay curves. They usually tend to have higher disagreement when the roll angle becomes small both for intact and damaged conditions. Fig. 6 confirms similar natural period and damping in roll when the draft is changed of about 20% for the intact ship section (see quantitative results in table 10). Fig. 7 illustrates that the roll motion dies out quicker for a ventilated damaged condition than for the airtight damaged compartment. Fig. 6 and 7 show an increase of natural period and damping in roll when going from intact to damaged ship (with the same loading condition both with ventilated and airtight conditions). Fig. 8 confirms that as the damage opening size reduces, the damping effect of internal floodwater decreases. One important thing to note is that the natural period for a damaged section decreases slightly as the roll angle becomes smaller. This may be because of the transient dynamic effect of floodwater, which is not accounted for in our theoretical estimates. Also, the damping for the first

Table 10
Natural period for roll and linear and quadratic damping coefficient.

Condition	Natural Roll Period T_{n4} (s)	Linear Damping Coefficient B_{44} (kg m^2 s^{-1})	$B_{44}^* = \frac{B_{44}}{\rho B^3 L T_d}\sqrt{\frac{B}{2g}}$	Quadratic Damping Coefficient $B_{44,quad}$ (kg m^2 rad^{-1})	$B_{44,quad}^* = \frac{B_{44,quad}}{\rho B^3 h_d d}$
Intact Draft 7 cm	0.92	0.63	0.78	0.4	–
Intact Draft 8.5 cm	0.94	0.6	0.62	0.4	–
Damaged Opening 1	2.45	1	0.567	2.86	1.98
Damaged Opening 2	2.46	1.02	0.578	2.29	2.12
Damage Opening 3	2.43	1.02	0.578	2.0	2.78
Damaged in airtight condition (Opening 1)	2.6	0.8	0.453	1.15	0.8

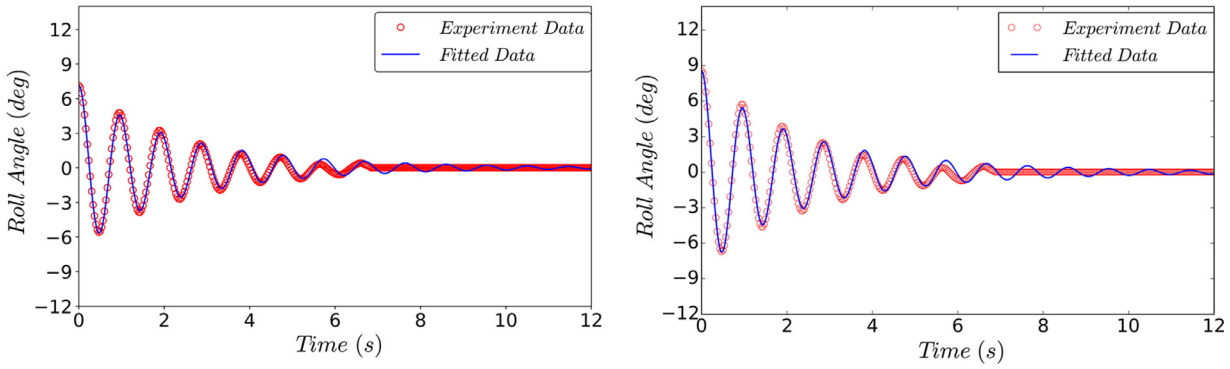

Fig. 6. Time history of roll angle of an intact section at 7 cm draft (left) and 8.5 cm draft (right).

oscillation period is much higher as compared to the other periods.

In the following sections, the behavior in waves of intact and damaged ship sections is examined. One should note that here we considered intact and damaged ship sections with the same loading conditions. This is consistent with analyzing the change in seakeeping when an intact vessel is suddenly damaged. Therefore, the draft of the examined damaged model is much higher than that of the corresponding intact model. Vugts [44] has demonstrated that the draft can affect greatly the roll added mass and damping coefficients. To highlight the pure effect of the opening on the hydrodynamic coefficients, the added-mass and damping coefficients for the damaged ship could be compared against those of an intact ship with the same draft. This has not been examined here.

6.2. Intact condition in beam-sea waves

Tests in beam-sea waves with wave steepness kA = 0.033 were performed for the intact section at two loading conditions corresponding to two different drafts. Figs. 9-11 show the RAOs for sway, heave and roll at the two experimental drafts, as well as the viscous strip-theory results for the 8.5 cm draft.

For the roll motions, both numerical and experimental results at draft equal 8.5 cm document a peak near a non-dimensional frequency of 1, which corresponds to a roll period of 1 s. This is consistent with the free-decay tests documenting a roll natural period of 0.94 s for this draft. A slight shift is usually observed due to sway-roll coupling as the free-decay tests assume a 1 DOF system. The natural roll response for the 7 cm draft is also close to 1 s, as seen from Fig. 11. The resonant roll response is higher for draft of 8.5 cm due to the smaller damping. Consistently with the expected asymptotic behaviors, the motions approach zero for high frequencies due to decreasing wave excitation, whereas at smaller frequencies, the non-dimensional motion values tend to a value of 1. The latter theoretical small-frequency sway result assumes infinite water depth.

The comparison with viscous strip theory seems reasonable for all RAOs, except near the roll resonance frequency where the theory shows an overprediction up to about 30%. Since the free roll decay tests show a small nonlinear damping, we have not included an equivalent linearized damping term for the intact case. The numerical method is able to capture the natural roll period, but the estimated damping seems to be smaller for roll and, due to roll-sway coupling, this affects also the sway motion.

6.3. Damaged condition in beam-sea waves

Full compartment flooding: We discuss results for the case when the compartment is damaged on the side facing the wavemaker and the damaged compartment encompasses the whole breadth of the model and is ventilated. Corresponding hydrostatic characteristics are illustrated in table 2. This table shows that due to the intact regions at the ends, we still have a reasonably high value of GM in damaged condition, which is maintained so that capsizing does not take place in all wave conditions examined. We first present the results for a damaged model draft of 15.5 cm with damage opening 1, corresponding to intact model draft of 8.5 cm.

Fig. 12 shows wave elevation RAOs inside the damaged compartment. The vertical dotted lines in the plots indicate the sloshing and piston-mode resonance frequencies. The largest measured wave elevations occur at higher frequencies with a maximum at WP1 of about 1.5 times the incident wave amplitude. At high frequencies, incident waves do not cause large heave or roll motion. However, due to the damage opening, an external forcing exists, which excites resonance inside the flooded compartment. The wave RAOs are small at the second sloshing mode (Figure 13) because the wave probes are located far away from crest or trough of the sloshing mode. Near the second piston mode frequency, we notice a large peak for both WP1 and WP2

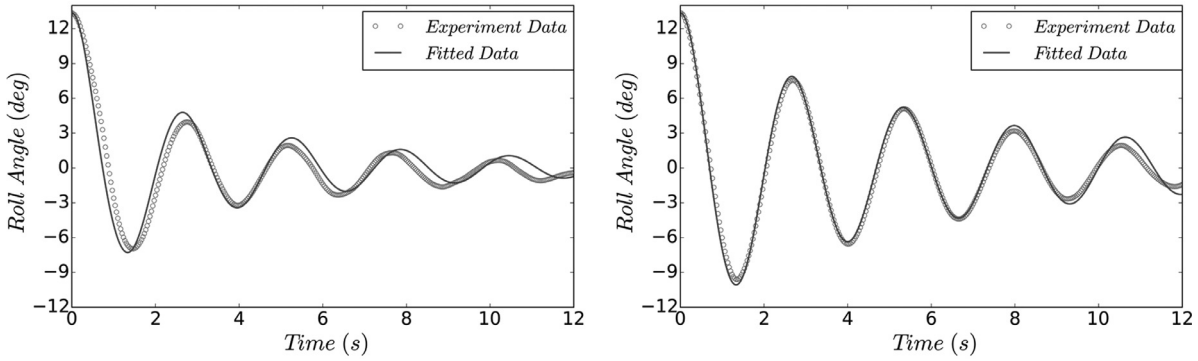

Fig. 7. Time history of roll angle for damaged section (left) and damaged section with airtight compartment (right) both at 15.5 cm draft with inflow/outflow thorough the damage opening.

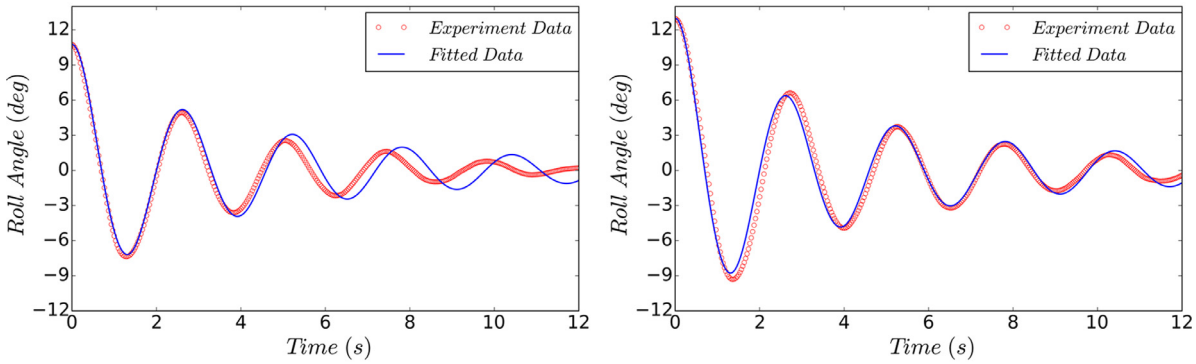

Fig. 8. Time history of roll angle for damaged section with Opening 2 (left) and damaged section with Opening 3 (right) both at 15.5 cm draft with inflow/outflow thorough the damage opening.

measurements. The piston mode and roll motion act as a coupled system causing high wave elevation values inside the compartment. The values for WP1 are higher than for WP2 since the crest is closer to WP1 than WP2. At $\omega^* = 0.91$, the first sloshing mode is excited (Fig. 14). At small frequencies, we see a small peak near the first piston mode frequency (Fig. 15). Five repetitions are performed for full compartment damage at 15.5 cm draft at six frequencies and two wave steepnesses. Error bars in the plots show the absolute deviation with mean values at the wave probes. The deviation for WP2 is small and less than 15% for all cases. For WP1, the maximum deviation is higher, around 20%.

Figs. 16-18 provide the experimental sway, heave and roll RAOs for full compartment flooding at two steepnesses and the comparison with viscous strip-theory results. All motions are small at high frequencies just as for the intact model. Higher frequencies can excite higher sloshing modes inside the damaged compartment but do not cause large body motions. At smaller frequencies, the behavior is different as compared to an intact section with larger sway motions occurring in this case. Heave motion shows slightly larger values near the first piston mode frequency as compared to the intact model. Roll RAO is very different when compared to an intact section. A special feature of roll RAO for a damaged ship section is that it has usually two peaks, i.e. a peak at the natural roll period for the damaged section and a minor peak close to the first sloshing mode resonance period. The natural roll period for the damaged ship section is calculated to be 2.43 s ($\omega^* = 0.41$) and matches quite well with the main peak in roll RAO. The roll damping calculated from the experiments is higher for the damaged section when compared to the intact section, as previously discussed. However, the roll response at the natural period for the damaged section is higher than for the intact section. In general, most experimental literature shows that the roll response for damaged condition is lower than for intact condition. We must, however, note that experiments for the whole ship experience a more limited change in draft due to flooding with respect to our case. In our case, the draft and natural periods are almost doubled when going from intact to damaged scenario. Therefore, even though the absolute value of roll damping is higher for the damaged condition, the exciting roll moment from the waves at the much smaller frequency may be large enough to cause a net larger response for the damaged ship. Sway, heave and roll motions show mostly linear behavior. Some nonlinearity is observed for the smallest wave steepness, which may be connected with error in the measurement for small motions. Furthermore, calculations show that nonlinear viscous damping matters at roll resonance. The two examined wave steepness values may not be large enough to cause significant nonlinear behavior. Error bars show absolute deviation with mean values of the motions. The deviation is usually less than 10% for sway and heave at both steepnesses. The deviation is a bit higher for roll RAO with a maximum value of 19%. The overall repeatability of the tests is in acceptable range with maximum deviation for all RAOs below 20%.

The comparison of experimental data with numerical results is good except for the roll response at certain frequencies. A possible explanation of the difference between experimental and strip theory results is that 3D effects due to change from intact to damaged 2D cross-section at the opening is not accounted for by strip-theory. Furthermore, since 2D flow is assumed for the radiation and diffraction problems for the damaged strip, we cannot account for possible 3D floodwater effects.

To quantify the influence of nonlinear roll damping on the roll motion, especially near resonance, the roll damping in the motion equations (1) is defined as

$$B_{44,tot} = B_{44l} + \frac{8\omega}{3\pi} B_{44,quad} \eta_{4a} \tag{3}$$

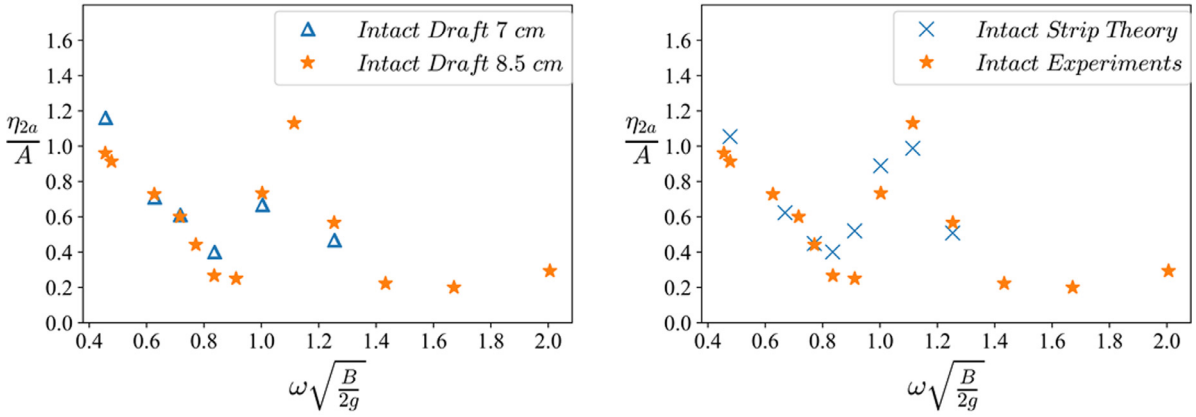

Fig. 9. Experimental sway RAO as a function of frequency for the intact section at two drafts (left) and comparison with viscous strip-theory results for 8.5 cm draft (right).

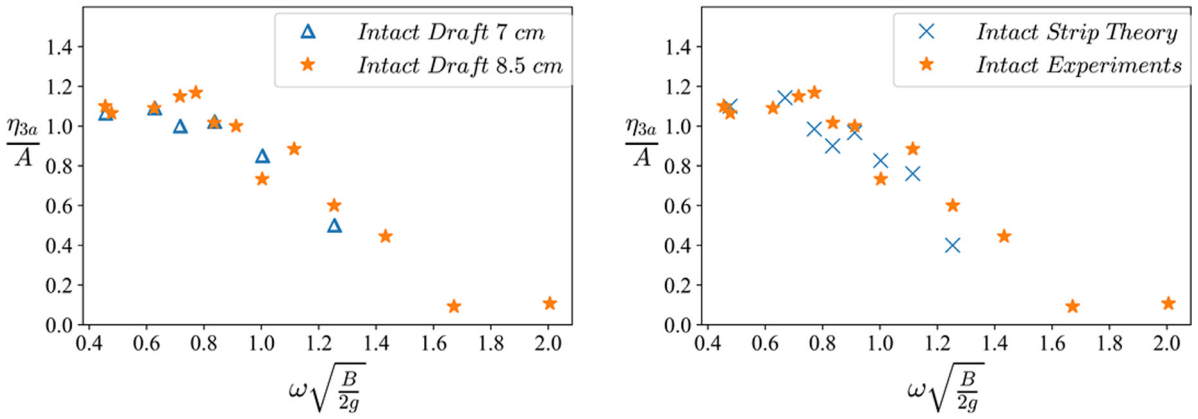

Fig. 10. Experimental heave RAO as a function of frequency for the intact section at two drafts (left) and comparison with viscous strip-theory results for 8.5 cm draft (right).

Here, B_{44l} is the linear roll damping, $B_{44,\ quad}$ is quadratic roll damping used in an equivalent linear formulation (Faltinsen [45]), ω is the incident wave frequency and $\eta_{4a}$is the roll amplitude in radians. B_{44l} and$B_{44,\ quad}$ are calculated with OpenFOAM by simulating two radiation problems in roll at oscillation frequency ω and with two different forced-roll amplitudes. In particular, they can be estimated using a linear fitting curve of the roll-damping results from the two simulations. Because $B_{44,\ tot}$ depends on the roll amplitude, we must solve the equations of motion (1) iteratively until the roll amplitude used for estimating the damping in eq. (3) gives the same roll amplitude for the next iteration. The obtained damping shows good agreement with the damping from the free roll decay tests.

The piston and sloshing mode resonances affect the body motions. For the damaged section in beam-sea waves, the major roll peak is located near the first piston mode frequency as seen in Fig. 18. This is a simple consequence of the restoring roll moment C_{44} being greatly reduced leading to a larger natural period. This period happens to be close to the first piston mode because the internal free-surface at natural roll period inclines along with the section (with a slight phase difference) resembling a piston mode, i.e. an almost node like condition at the opening and an antinode at the opposite wall. The sway peak at roll natural period occurs due to coupling between roll and sway motions. Heave motion is mostly similar to an intact section except near first piston mode period which can be an effect of large mass inflow/outflow at natural roll period.

The influence of sloshing mode resonance on a damaged ship motions can be understood by comparing with the motions of a ship having an internal tank as discussed by Faltinsen and Timokha [31]. Rognebakke and Faltinsen [46] also studied experimentally and numerically the influence on a model (with closed internal tank) that was restrained to only move in sway motion in incident regular waves with frequencies in the vicinity of the lowest natural sloshing frequency. Since the contribution to sway added mass from sloshing becomes infinite at the sloshing natural frequency, the linear sway response becomes zero at the natural sloshing frequency. Furthermore, because of the strong frequency dependence of the sway added mass due to sloshing with large negative and positive values in the vicinity of the natural sloshing frequency, a maximum in sway response occurs at a frequency slightly higher than the lowest natural sloshing frequency. If the body with an internal tank is free to move in all rigid-body degrees of freedom, the motions in general will not be zero at the natural sloshing frequency. The latter is the consequence of hydrodynamic coupling properties and is proved by Faltinsen and Timokha [31]. Due to sway-roll coupling, at the first natural sloshing frequency, a dip occurs for the roll RAO and a nearby peak at frequency lower than the sloshing frequency is observed. Following this, for our case, we do not observe very large motions at sloshing resonance, but a small minor peak for roll and small dip in sway motion occur near the first sloshing mode resonance frequency. This is similar to the behavior described for a body with closed internal tank in beam-sea waves, but the effect is not as large in our case. To demonstrate a case where the effect of sloshing resonance appears more clearly, we refer to experiments on a damaged model in beam-sea waves by [24]. They presented motion RAOs for experiments on a ferry hull model in intact and damaged condition in beam-sea waves for side damage, bottom damage and floodwater with the opening closed (behaving as an internal closed tank). For the damage compartment in their case, we calculate the sloshing resonance frequencies as described in Section 3 and the piston mode frequencies

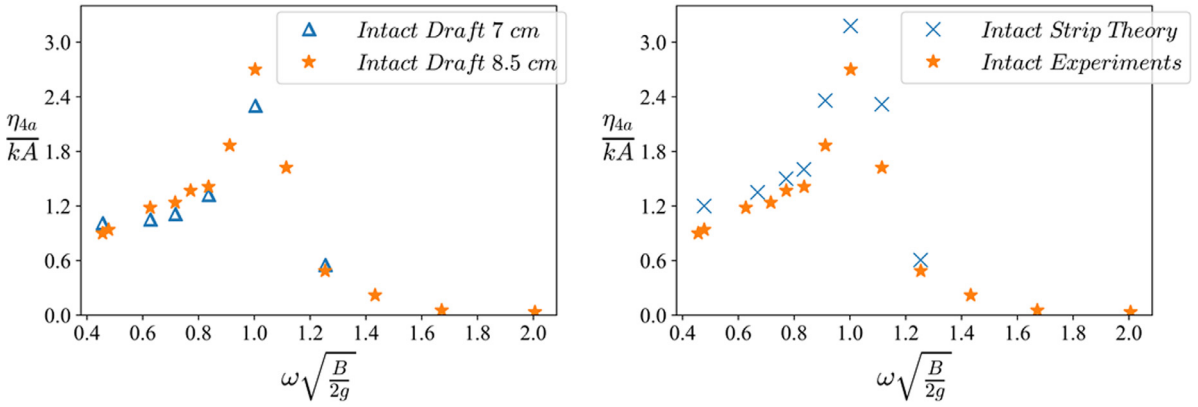

Fig. 11. Experimental roll RAO as a function of frequency for the intact section at two drafts (left) and comparison with viscous strip-theory results for 8.5 cm draft (right).

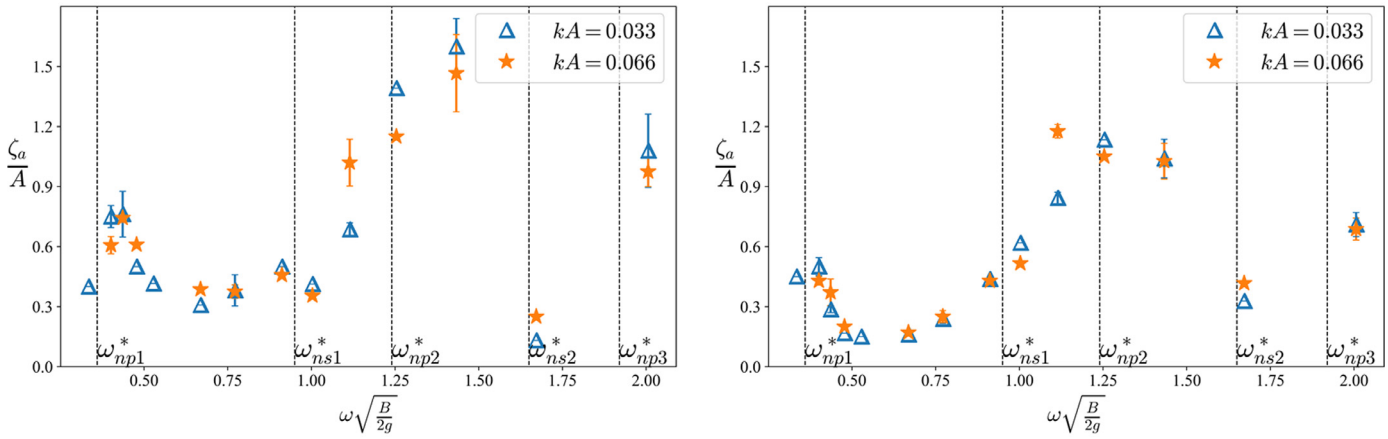

Fig. 12. Wave probe RAOs at WP1 (left) & WP2 (right) inside ventilated damaged compartment as a function of frequency for full compartment flooding (Opening 1) and two wave steepnesses.

using the formulation for a harbor by Miles and Munk [32]. Fig. 19 reproduces Fig. 15 from [24] with the predicted values of the sloshing and piston mode frequencies given by the vertical dotted lines. The calculated first piston mode frequency ($\omega^* = 1$) and second sloshing frequency ($\omega^* = 4.9$) are out of their examined range. We observe that two peaks in roll occur and the effect of first natural sloshing frequency is evident. Especially, the behavior for the case of flooding with closed opening (black line in figure 19) can be explained as discussed above for 3 DOF body motions coupled with sloshing due to an internal tank, similar to as seen in figure 3.26 in [31]. The two damage cases (side and bottom damage) follow similar behavior for this model.

Fig. 20 shows wave elevation RAOs inside the compartment at 11 cm draft, which corresponds to intact model draft of 7 cm. In this case, the free-surface level is below the upper opening edge and not bounded by a wall on the opening side. As the filling level in the damaged compartment is smaller, the sloshing and piston mode frequencies are modified. We see a large peak around the second piston mode and third piston mode, this behavior of wave systems at smaller filling depth is discussed in Siddiqui et al. [1]. Figs. 21 and 22 show the second sloshing mode and second piston mode being excited in the compartment for this case.

Fig. 23 shows sway, heave and roll RAOs for full compartment flooding at 11 cm draft. Sway behavior is significantly changed as compared to the 15.5 cm flooding scenario in Fig. 16 (referred to as higher filling level in this section). We see a large peak between the second piston and second sloshing mode frequencies. Heave motion shows similar behavior as for the higher filling. Heave natural resonance period is governed by the waterplane area, which is the same for both damage cases. Therefore, we expect similar heave behavior for both filling levels. Roll motion is significantly modified and as seen earlier, presents a strong coupling with sway motion. We observe a peak near the second piston mode frequency and one smaller peak approaching the first piston mode. The RAO value near the first piston mode frequency is much smaller compared to the higher filling level. This may be because roll damping is larger due to higher beam to draft B/T ratio in this case and also because the wave system inside the damaged compartment is modified. Near the second piston mode, the roll motion is slightly larger than for the higher filling level.

6.3.1. *Effect of air compressibility in damaged compartment*

For an airtight compartment, the air compressibility in the damaged compartment acts as a strong spring and influences water inflow/outflow through the opening and, therefore, the motion responses. Air in the compartment slows down the flooding process as mentioned in [27] and [28]. When air cavities are involved, we must consider if Euler number $Eu = p_a/\rho U^2$ matters in scaling from model tests to full scale (Faltinsen and Timokha [31]). Here p_a, ρ and $U$are ambient air pressure, water density and characteristic velocity, respectively. Since Froude scaling is applied, Euler number scaling implies that depressurized conditions are needed in the model tests. Existing wave flumes do not allow for such an investigation, in general, but Ypma [47] has presented experiments for a damaged scenario in vacuum conditions. To avoid the problem of using depressurized conditions, Ruponen et al. [28] performed experiments on a full-scale ship to study the effect of air cavity on flooding to circumvent the problem of scaling air stiffness from model to full scale. They concluded that air compression can slow down initial flooding largely and therefore can have a significant effect on ship motions. Air compressibility may be therefore important even in real-ship scenarios if the air-pipe vents are small or flooded. In the present scenario, this effect has been investigated experimentally by sealing all air exits and openings for the full compartment damage.

Fig. 24 shows wave elevation RAOs inside the compartment for

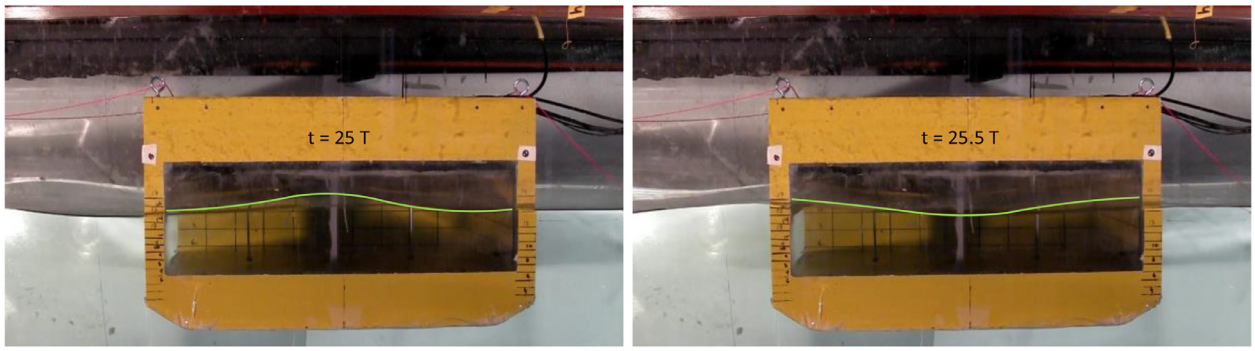

Fig. 13. Second sloshing mode for ventilated condition with damage opening 1 (left side of model) in waves at kA = 0.033 and ω^*=1.667.

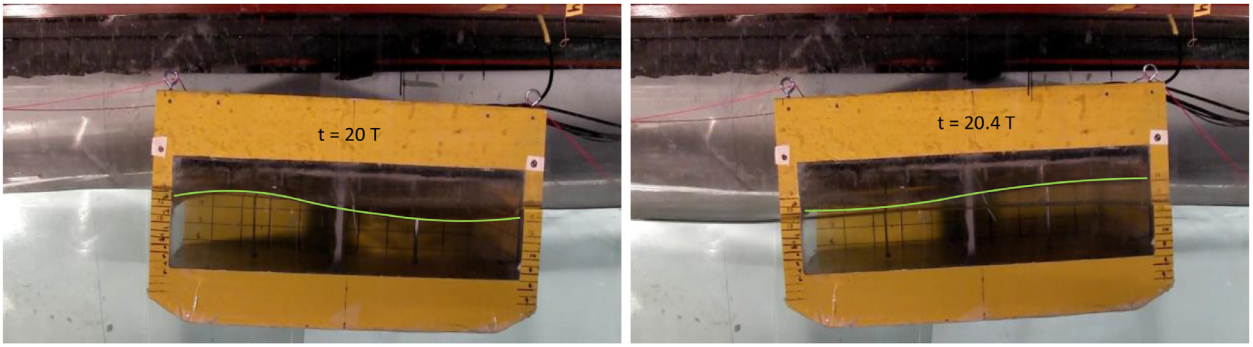

Fig. 14. First sloshing mode for ventilated condition with damage opening 1 (left side of model) in waves at kA = 0.033 and ω^*=0.91.

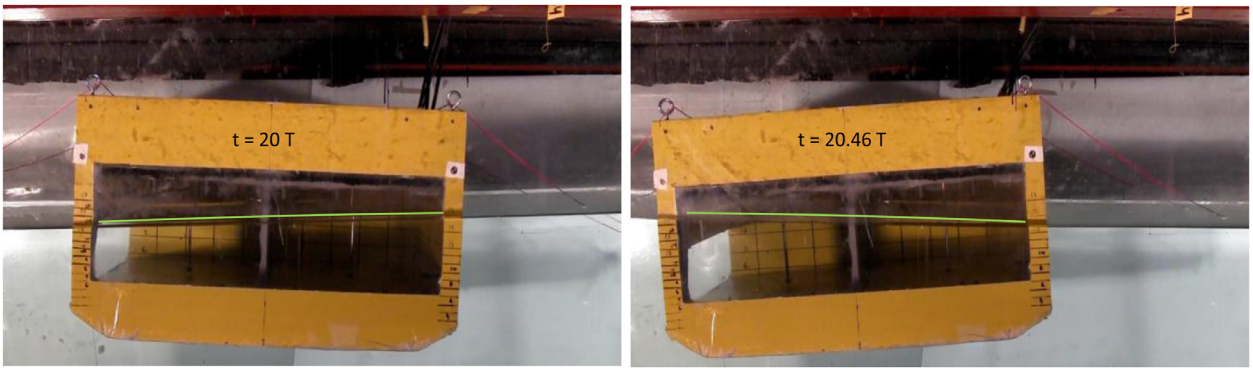

Fig. 15. First Piston mode for ventilated condition with damage opening 1 (left side of model) in waves at kA = 0.033 and ω^*=0.33.

ventilated and airtight conditions. Due to the air cushion acting as a spring, the wave elevation values for WP1 and WP2 inside the airtight compartment are lower as compared to the ventilated compartment. This effect is more pronounced at larger frequencies as compared to smaller frequencies. Fig. 25 shows sway, heave and roll RAOs for ventilated and airtight compartments. Sway motion is not greatly affected by the air compressibility. Heave motions are highly modified due to the air cushion especially near $\omega^* = 1$. The motions are much larger at this frequency as compared to a ventilated compartment. The roll RAO shows a similar trend as for the ventilated compartment. The only difference being that the motions are larger near the natural roll frequency. This is because of smaller roll damping at roll resonance for the airtight compartment as demonstrated earlier in Section 6.1. [1] documents that piston mode resonance is absent for an airtight compartment for forced heave motions whereas, sloshing resonance remains unaffected. WP1 values show reduction in values near the piston mode frequency in this case but not as small as in [1]. This can be because [1] documented a 1 DOF system in heave motion, whereas, in this case, we study a freely floating 3 DOF system. For approximation of heave resonance frequency, we consider a single DOF system in forced heave motion as in [1]. The restoring coefficient C_{33} is because of change in vertical force due to quasi-steady change $-\rho g \eta_3$ in hydrostatic pressure. We neglect the effect of the thin vertical walls. Since the pressure can be assumed constant in the air cushion and the pressure at the interface between the air cushion and water must be equal, there is a change of pressure equal to $-\rho g \eta_3$ in the air cushion. This pressure acts on the lower deck of the model at the upper interface between the air cushion and the model. If we sum up the contribution due to change of hydrostatic pressure, we find the same 2D restoring coefficient for the airtight damaged section as for the intact section. It means that for

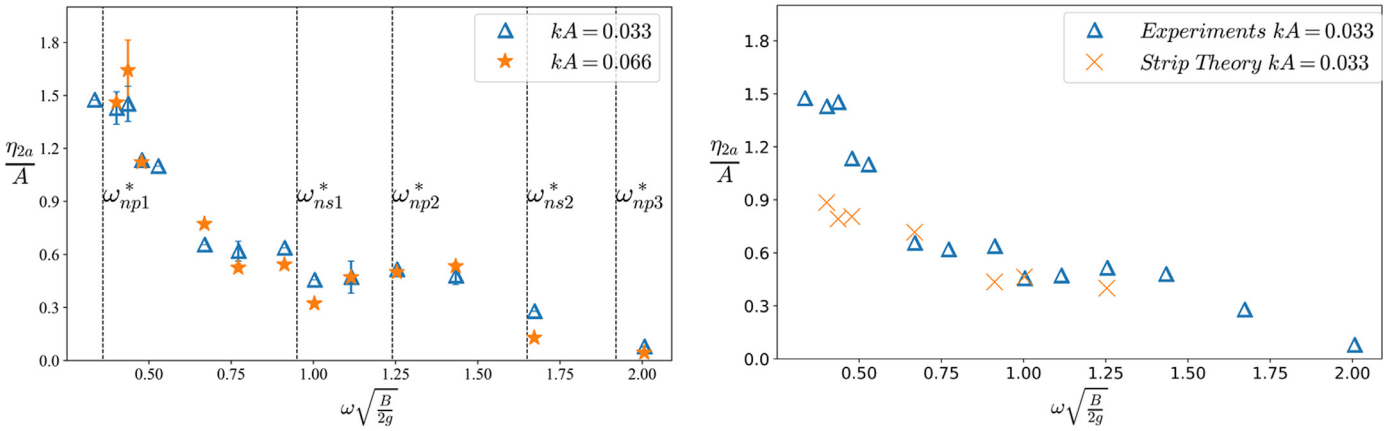

Fig. 16. Sway RAO as a function of frequency for ventilated full compartment flooding (Opening 1) and two wave steepnesses (left) and comparison with viscous strip-theory results (right).

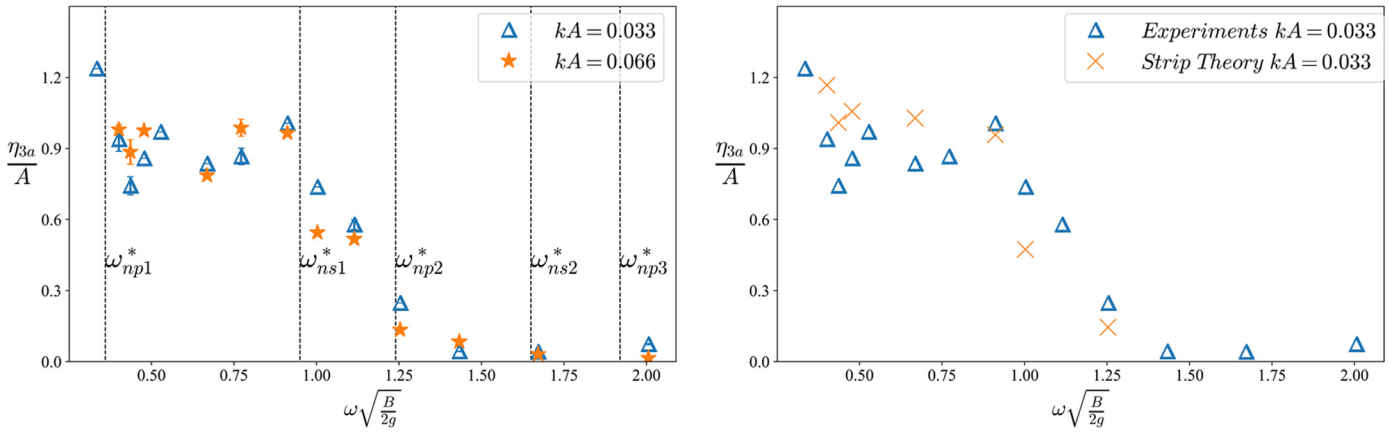

Fig. 17. Heave RAO as a function of frequency for ventilated full compartment flooding (Opening 1) and two wave steepnesses (left) and comparison with viscous strip-theory results (right).

airtight case $C_{33} = \rho gBL$. There is contribution to the added mass from the internal and external flow. One contribution to heave added mass from the internal flow is simply the internal water mass. A first approximation of the external contribution to the heave added mass is that the sectional heave added mass is proportional to B^2, i.e. the same as for the intact section. The consequence is that the natural frequency for the damaged model with air cushion is $\omega^* = 0.94$. [1] documented in Fig. 37 heave added mass and damping for ventilated and airtight sections, which demonstrated that damping is higher for ventilated damaged section as compared to an airtight damaged section. Therefore, we see higher values of roll motion for the airtight section. Similar argument can be made for the roll restoring coefficient C_{44} as shown in section 5.3 (Faltinsen [42]) for a surface effect ship (SES).

6.3.2. Effect of damage-opening size

To study the effect of damage-opening size on the motions, three opening sizes were studied. The dimensions of the openings are described in table 5. Additional thin wooden plates were attached at the sides to reduce the opening length for Openings 2 and 3. Fig. 26 shows the wave elevation RAOs inside the compartment for the three different opening sizes. All the three openings document similar trends as shown in Fig. 12. The RAOs of WP1 and WP2 for Opening 2 and 3 are mostly similar or smaller than the values for Opening 1. This is understandable as the inflow/outflow for the smaller openings is more restricted. It is, however, interesting to note that the values for the smaller openings are slightly larger near the first piston mode frequency.

Fig. 27 shows sway, heave and roll RAOs for the three damage-opening sizes. The behavior for the three openings can be divided into two types of sections. The first type is the smallest opening (Opening 3) which behaves closer to a closed tank and is less affected by piston mode and associated damping. The reason is that cross-sectional parts of the damaged compartment is closed, and piston-mode resonance cannot occur there from a 2D flow point of view. The other type is for the largest opening (Opening 1), which has large inflow/outflow due to piston mode resonance and therefore, larger damping. The sway behavior is mostly similar for all the three cases. However, near the first sloshing mode, as the opening size becomes smaller, we see a reduction in sway motions. This can be because the smaller opening compartment partly involves cross-sections with closed internal 2D tank. This matters especially at sloshing resonance. As mentioned earlier, sloshing due to an internal closed tank reduces the sway motion considerably for a 3 DOF system. Heave motions displays a similar trend for the three openings except at a few frequencies. Roll RAO values are also similar except at roll resonance frequency. The value for the smaller openings is larger due to the smaller total damping as shown in Section 6.1.

6.3.3. Half compartment damage

Experiments have also been performed on the model with damage only extending to half of the initially described compartment. A watertight plate was placed at the center plane of the compartment for this case. The damaged region is now asymmetric with respect to the z-axis and leads to an initial equilibrium condition with non-zero heel angle (Fig. 28). Two drafts corresponding to intact model draft of 7 cm and 8.5 cm are studied in this case. For the damaged condition, this leads to

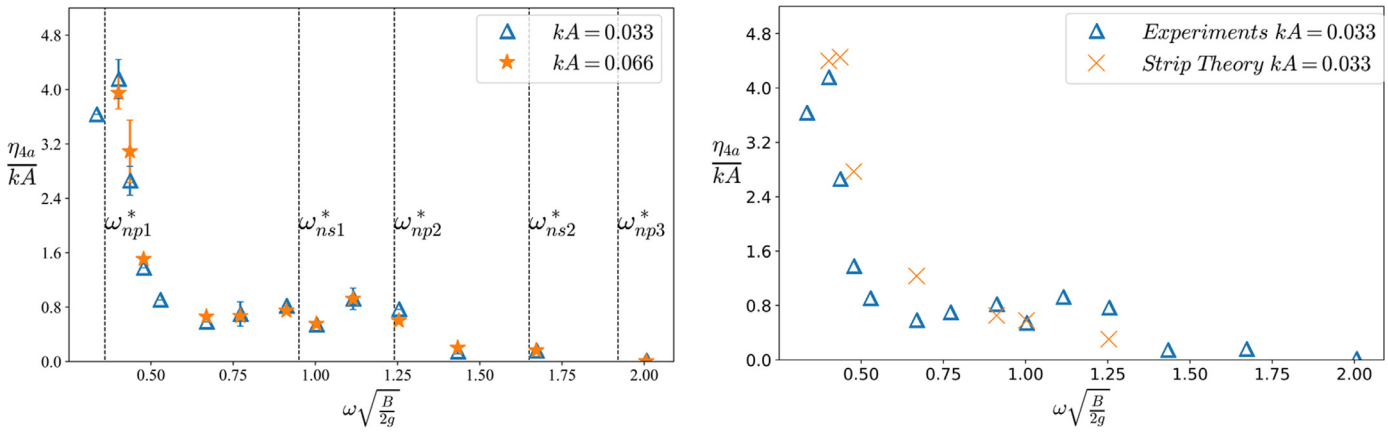

Fig. 18. Roll RAO as a function of frequency for ventilated full compartment flooding (Opening 1) and two wave steepnesses (left) and comparison with viscous strip-theory results (right).

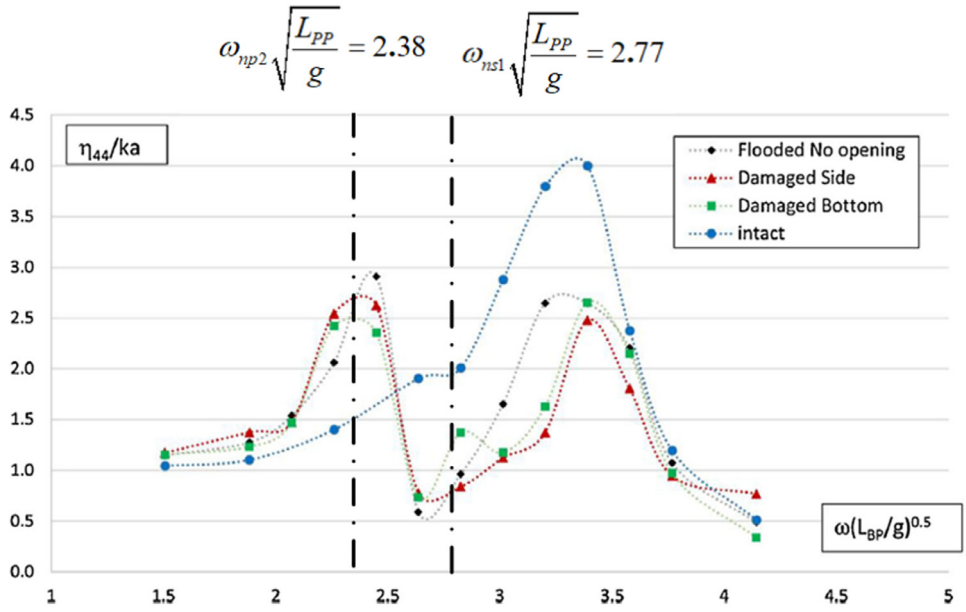

Fig. 19. Fig. 15 from [23] along with marked the sloshing and piston mode resonance frequencies (here LBP is LPP (length between perpendiculars) and η_{44} is same as η_{4a} in present work).

drafts of 12.5 cm and 16.5 cm, respectively, towards the damaged side. In this section, we refer to the two cases using these two draft values. Since the breadth of the compartment is halved, the sloshing and piston mode frequencies are now much higher with only the first sloshing and piston mode lying within the range of examined frequencies.

Fig. 29 shows RAOs of heave and wave elevation at one steepness for 16.5 cm draft and 12.5 cm draft (Opening 1 and 3). In the figure, the subscript *d* and *s* in the natural frequency refer to the 16.5 and 12.5 cm cases, respectively. Heave RAO is mostly similar for the three cases, except for small differences near the roll resonance frequency ($\omega^*=0.91$). For 12.5 cm draft with the smaller opening, heave values are slightly larger. The wave elevation RAO does not display a sharp peak for the 16.5 cm case. The first sloshing mode is observed (see Fig. 30) but with very small wave RAO values, since the WP lies at the node. The wave elevation in the 12.5 cm case shows larger values, since in this case travelling waves occur (see Fig. 31). A large crest rises at the opening and is reflected as a large 'hump' by the non-damaged opposite wall. This can also cause large sway forces. For smaller opening, we see a similar trend with slightly lower values.

Fig. 32 shows sway and roll RAOs at one steepness, for 16.5 cm draft (Opening 1) and 12.5 cm draft (Opening 1 and 3). The sway behavior is similar for the three cases, except near roll resonance. This can be explained due to occurrence of travelling wave systems for the smaller submergence at these frequencies. The roll motion shows a peak at a non-dimensional frequency of 0.9, which seems to be the natural roll period for this case. This lies between the first piston and sloshing mode frequencies. We must note that there might be an error in the calculation of the piston mode frequency, as for simplicity we have assumed that the heel angle will not affect the natural piston mode resonance. This is proven to be true for sloshing by Faltinsen and Timokha [31] but may not hold for piston mode resonance. Also, as expected due to the initial heel angle, the motions are highly damped compared to the full compartment damage case. The roll motions are, in general, similar for the two submergence cases, except near the roll resonance. At higher submergence the peak is sharper compared to the smaller submergence. By a sharp peak, we imply that the slope of roll RAO for the smaller submergence values is higher between $\omega^*=0.91$ and $\omega^*=1.25$ as compared to the higher submergence. For the 12.5 cm draft, reduced opening size leads to a slightly larger roll motion at resonance. This is because the damping is smaller for the smaller opening size as discussed earlier for the full compartment damage.

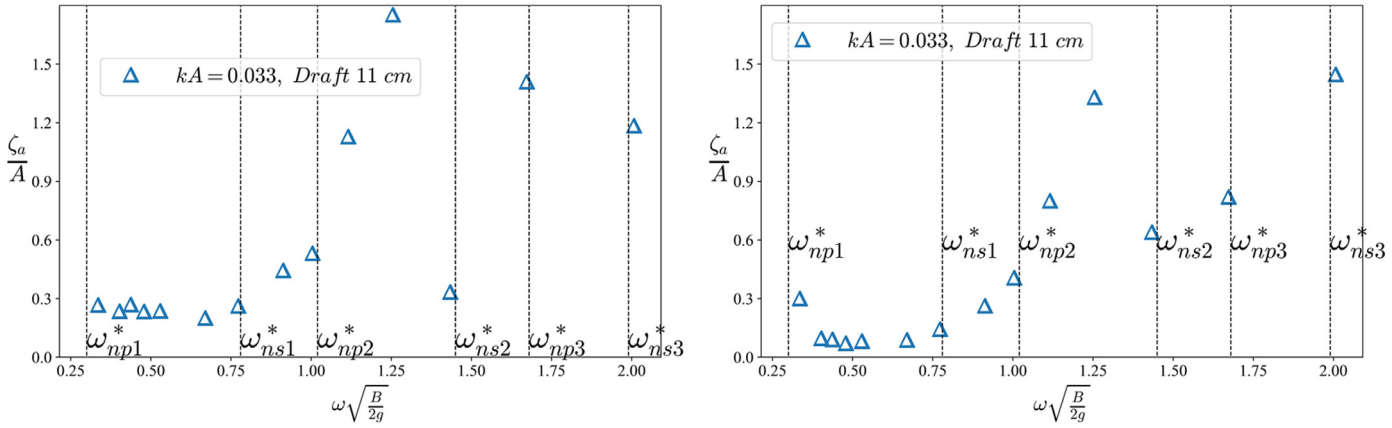

Fig. 20. Wave probe RAOs at WP1 (left) & WP2 (right) inside damaged compartment (Opening 1) as a function of frequency for full compartment flooding at 11 cm draft.

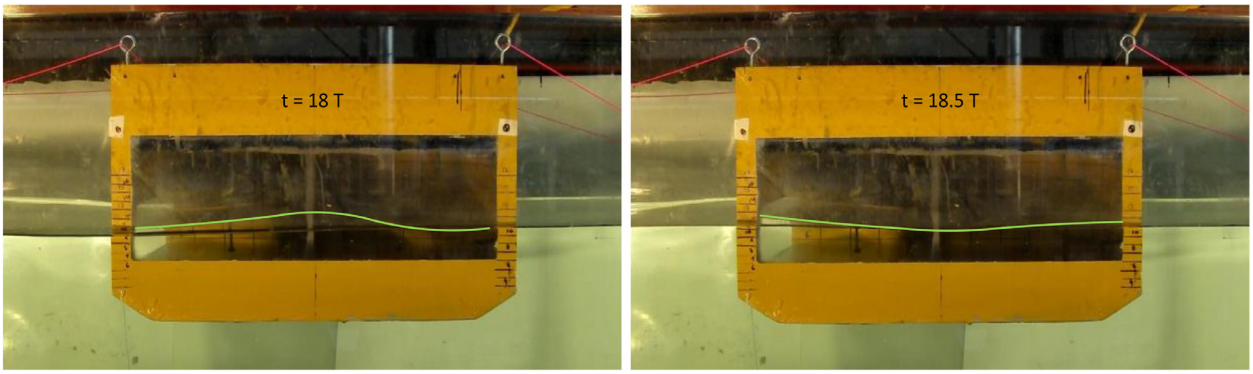

Fig. 21. Second sloshing mode for a damaged model (Opening 1) in waves at kA = 0.033 and ω^*=1.5 and 11 cm draft.

6.4. Transient flooding

The transient flooding stage occurring immediately after a damage event, when the ship is exposed to incident waves, is very important as the largest motions take place in this stage and subsequent capsizing may be experienced. In the present tests, we tried to examine situations when initial transient flooding occurs due to the motions of the ship. This can be the case when the damage opening is located above the initial waterline draft of the ship and is not sealed to external environment, like in the case of Estonia accident. Such a scenario was studied experimentally for bow flooding by Shimizu et al. [48]. They varied Froude number, wave period, wave height and bow opening size and reported that the wave height and wave periods were the dominant factors in determining flooding. A similar aspect has been investigated here but for a half compartment with side damage in beam-sea waves. The transient flooding is examined by varying three parameters i.e. KG, incident wave period and incident wave steepness. The examined model loading conditions are described in table 11. In particular, the loading GM1 was used as basis to investigate the influence of incident wave steepness, ranging between 0.033 and 0.1, and incident-wave period, ranging between 0.7 and 1.5 s. Then the effect of the loading was studied for incident-wave steepness kA = 0.066 and incident-wave periods 0.8, 0.9 and 1 s. Enough freeboard height is allowed so that flooding does not occur for all studied incident periods and effect of varied parameters can be highlighted. The height of the opening edge of the compartment is increased using a small wooden plate 10 cm high from the bottom of the model leading to an initial freeboard of the opening edge of about 2.2 or 3 cm.

The case with the model in loading condition GM1 and incident waves with kA = 0.066 and period T = 0.9 s is used to describe the typical features of flooding in our tests. One should note, that in this case the roll natural period is 0.95 s before flooding. Fig. 33 shows sudden transient flooding leading to a large sinkage and heel angle. The motions increase in magnitude and just when flooding starts around t/T = 35, we see a jump in roll and heave motions. After the sudden jump, motions are large but stabilize around t/T = 50 to a new equilibrium level. These results document similar behavior as in the stages identified by Ruponen [2] and reported in Section 2.1 of his thesis.

Fig. 34 examines in detail the different stages of flooding for the same wave period and steepness. As the roll motion increases and gradually reaches a steady-state condition, the freeboard height of the opening relative to the external wave decreases and water starts entering the damaged opening. This inflow of water increases the model weight towards the damaged compartment and therefore increases the mean roll moment. The model tries to recover by rolling to the other side but the increase in roll moment towards the damaged side, coupled with reduction in GM due to the free surface in the compartment, further increases the roll motions. As a result, the magnitude of roll angle towards the damaged side increases over time and the model takes in more floodwater. The initial flooding may be slow for some incident wave-periods until when a sudden abrupt flooding occurs with sudden large transient motions.

For loading condition GM1, we studied cases with kA = 0.1 for four wave periods, T = 0.8,0.9,1 and 1.5 s. Flooding was observed in all cases, demonstrating that at very large values, the wave height becomes the primary factor for flooding. The two smaller steepnesses help us to examine the effect of other important parameters. Table 12 describes all examined flooding scenarios for kA = 0.033 and 0.066 at three loading conditions and different incident wave periods. We observe that shorter wave periods, relative to the natural roll period, with smaller wave amplitudes can cause flooding whereas longer waves with larger amplitudes may not cause flooding. Therefore, flooding depends not just on the wave height but also on the natural roll period of the ship model. This depends on the GM, and therefore, KG of the model. Longer waves cause larger heave motions, but smaller roll response and the ship tends to follow the waves. Thus, even with the opening near the waterline, flooding does not occur. The wave steepness kA = 0.033 is small enough to not cause flooding for any GM or incident wave period. For GM1, the

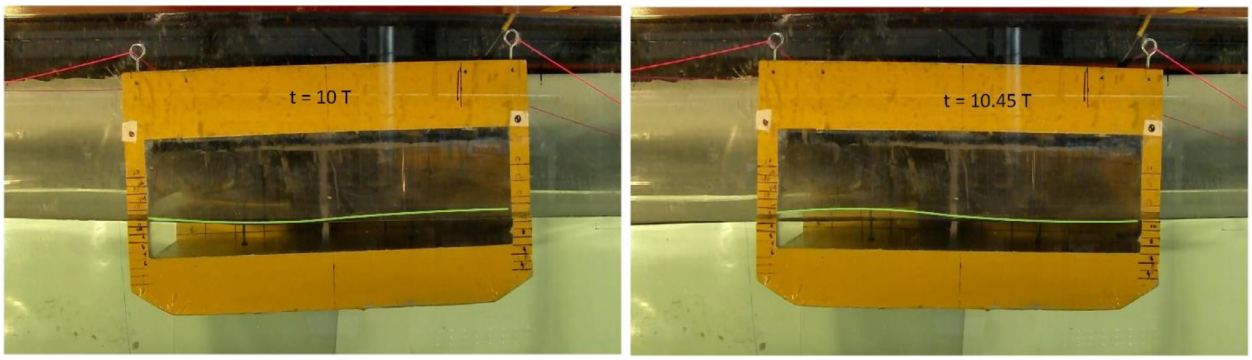

Fig. 22. Second piston mode for a damaged model (Opening 1) in waves at kA = 0.033 and ω^* = 1.11 and 11 cm draft.

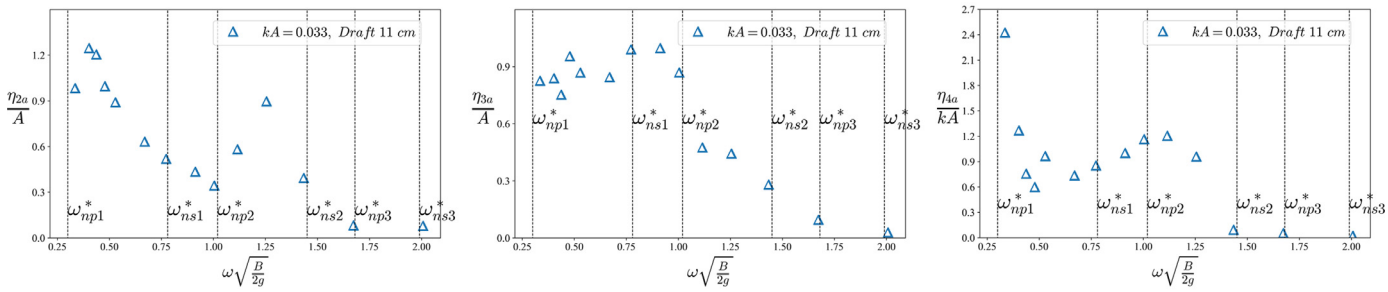

Fig. 23. Sway, heave and roll RAOs as a function of frequency for full compartment flooding (Opening 1) at 11 cm draft.

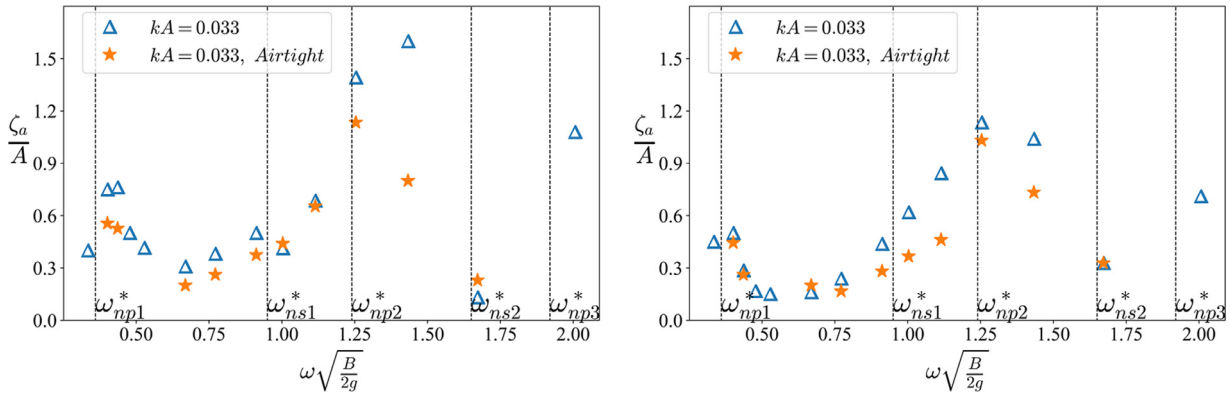

Fig. 24. Wave probe RAOs at WP1 (left) & WP2 (right) inside damaged compartment as a function of frequency for full compartment flooding in ventilated and airtight conditions.

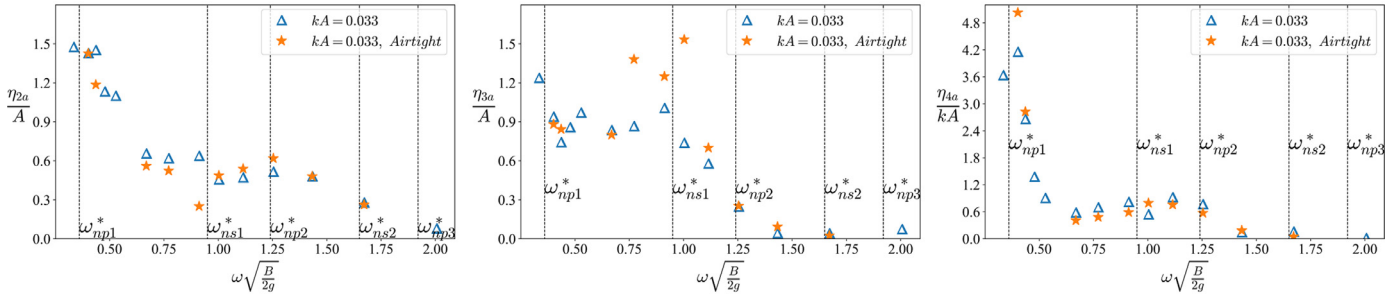

Fig. 25. Sway, heave and roll RAOs as a function of frequency for full compartment flooding in ventilated and airtight conditions.

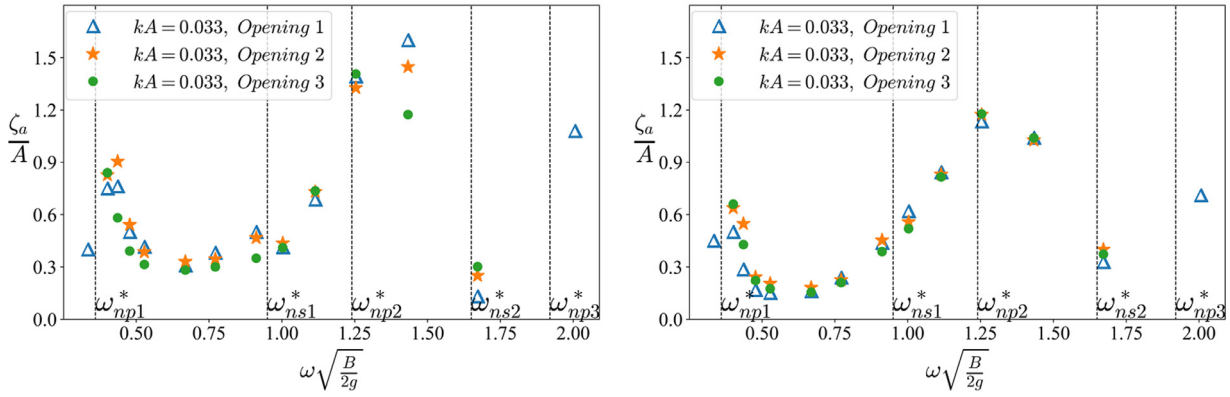

Fig. 26. Wave probe RAOs at WP1 (left) & WP2 (right) inside ventilated damaged compartment as a function of frequency for three damage-opening sizes.

roll natural period is around 0.95 s and therefore flooding occurs for $T = 0.9$ and 1 s at kA = 0.066. For $T = 1.5$ s, even though the wave amplitude is much larger than for $T = 0.9$ or 1 s, the roll motions are not large enough to cause flooding. As GM increases, the natural roll period as expected decreases. For loading condition GM3, all examined incident-wave periods are near the roll resonance period (0.89 s). Therefore, all these periods and kA = 0.066 cause flooding. The time t_{fl} in table 12 is defined as the time interval between beginning entry of

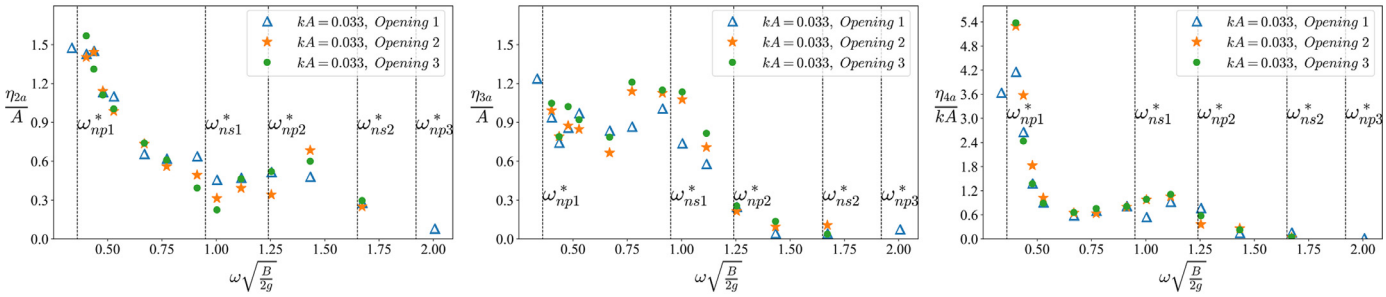

Fig. 27. Sway, heave and roll RAOs as a function of frequency for ventilated full compartment flooding at three damage-opening sizes.

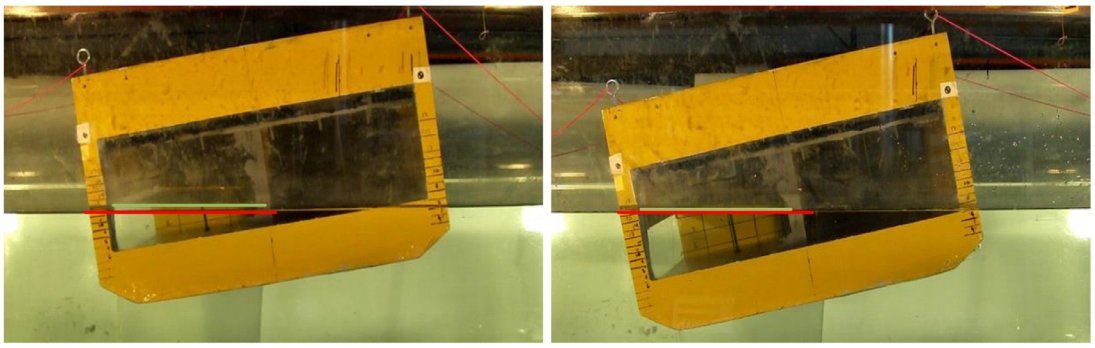

Fig. 28. Equilibrium position for half compartment damage at two drafts (green line indicates the internal free surface and red line indicates the outer free surface).

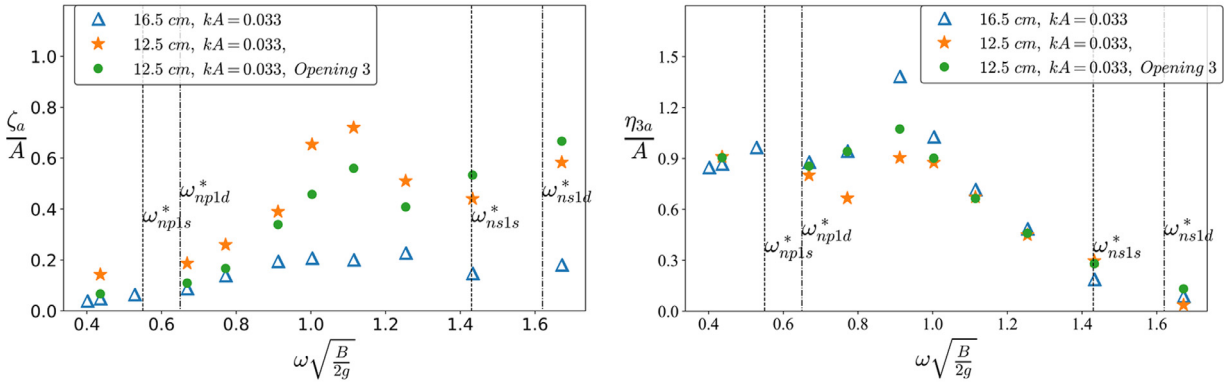

Fig. 29. WP1 and heave RAO for half compartment damage at 16.5 and 12.5 cm draft (two opening sizes).

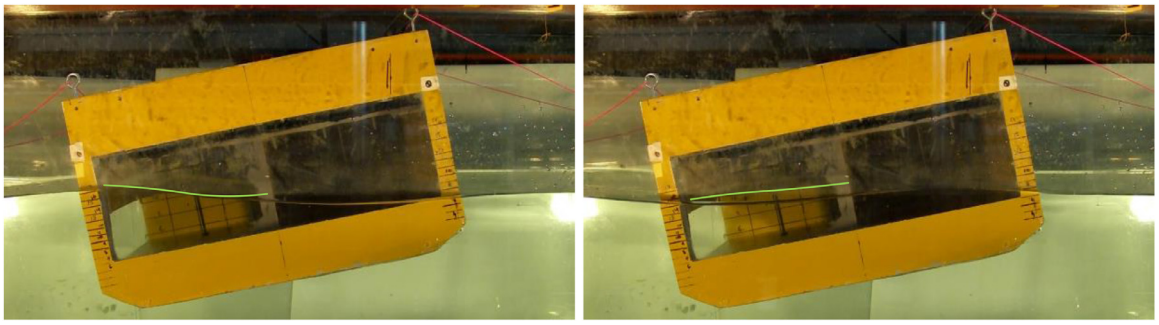

Fig. 30. First Sloshing mode in ventilated half compartment damage condition (16.5 cm, Opening 1) at kA = 0.033 and ω*=1.66.

flooding in the compartment to the attainment of final equilibrium position after flooding. In particular, the table gives the number of incident-wave periods within t_{fl} for the defined flooding time. As expected, the value is smallest for the incident-wave period closest to the roll natural period and increases going far from this period. One interesting observation is that for $T = 0.9$ s, GM1 with a higher freeboard has smaller values of t_{fl}/T than GM3 with a lower freeboard.

Fig. 35 shows the wave elevation inside the damaged compartment for the three flooding cases with loading condition GM3. Since the loading condition and initial draft are the same, we observe similar equilibrium floodwater level for the three incident-wave conditions. The difference in t_{fl} is clearly visible. Fig. 36 shows the wave elevation

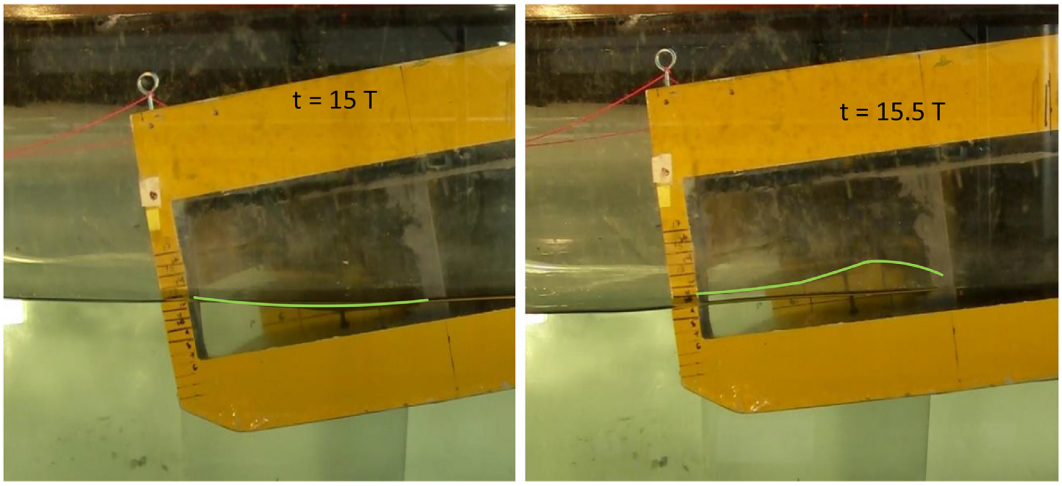

Fig. 31. Travelling waves in half compartment damage (12.5 cm, Opening 1) at kA = 0.033 and ω^*=1.11.

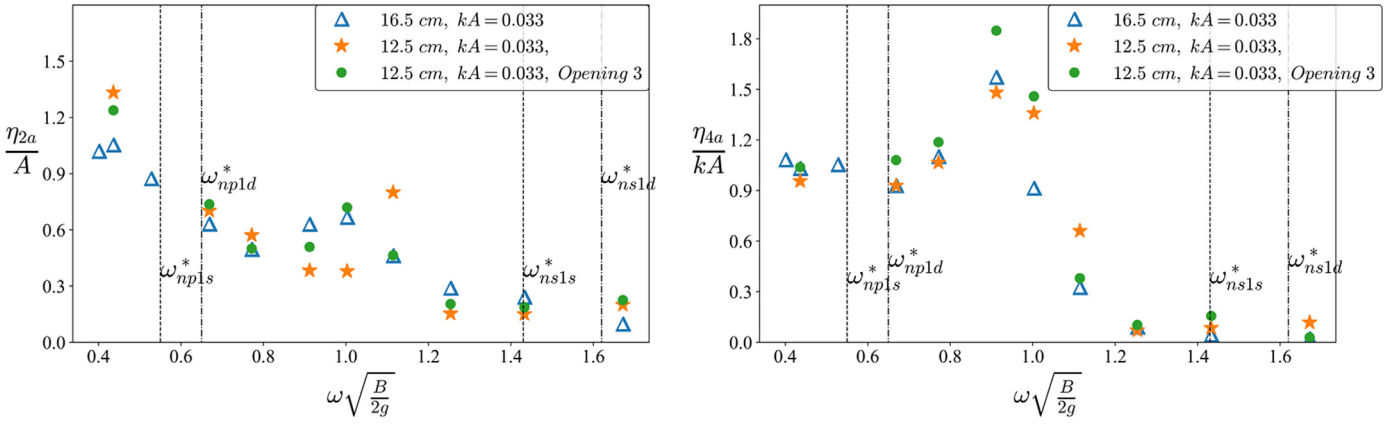

Fig. 32. Sway and roll RAO for half compartment damage at 16.5 and 12.5 cm draft (two opening sizes).

Table 11
Loading condition used for transient flooding cases.

Loading Name	Ballast (kg)	Draft (cm)	GM (m) before flooding	Freeboard (cm)	T_{n4} (s)
GM1	2	7	0.175	3	0.95
GM2	2	7	0.18	3	0.93
GM3	4	7.8	0.2	2.2	0.89

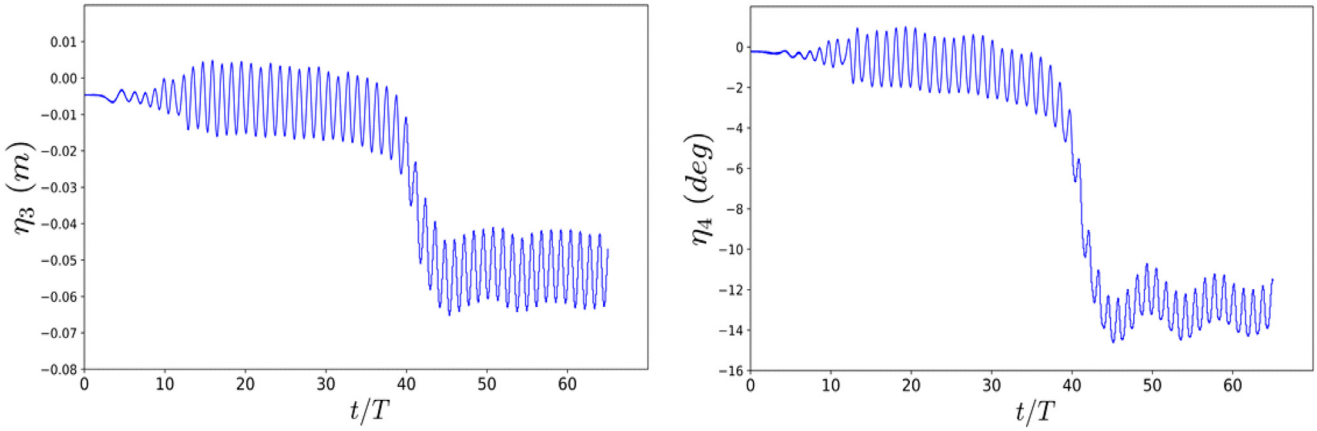

Fig. 33. Heave (left) and roll (right) time histories for the model in loading condition GM1 in waves with period T = 0.9 s, kA = 0.066.

Fig. 34. Sequence of flooding as it occurs over time for the model in loading condition GM1 in waves with period $T = 0.9$ s and kA = 0.066. Time increases from left to right and from top to bottom.

Table 12
Summary of flooding scenarios for the tests performed.

Period T (s)	Loading	Steepness (kA)	h_{fr} (cm)	Wave Amplitude (cm)	t_{fl}/T	T/T_{n4}	Remarks
0.7	GM1	0.033	3	0.45		0.74	
0.8	GM1	0.033	3	0.5		0.84	No Flooding
		0.066	3	1			No Flooding
0.9	GM1	0.033	3	0.65		0.95	Some splashes
		0.066	3	1.3	11.11		Flooding
1	GM1	0.033	3	0.8		1.05	No Flooding
		0.066	3	1.6	15		Flooding
1.2	GM1	0.033	3	1.1		1.26	No Flooding
		0.066	3	2.2			No Flooding
1.5	GM1	0.033	3	1.6		1.58	No Flooding
		0.066	3	3.2			No Flooding
0.8	GM2	0.066	3	1		0.86	Some splashes
0.9	GM2	0.066	3	1.3	12.8	0.97	Flooding
1	GM2	0.066	3	1.6		1.07	No Flooding
0.8	GM3	0.066	2.2	1	35	0.89	Flooding
0.9	GM3	0.066	2.2	1.3	17.77	1.01	Flooding
1	GM3	0.066	2.2	1.6	24	1.12	Flooding

in the half compartment for $T = 0.8$ s (left) and $T = 0.9$ s (right) at different loading conditions. For $T = 0.8$ s, flooding only occurs for the highest GM value i.e. GM3. Some water enters (green spikes) for GM2 but it does not cause further flooding. For $T = 0.9$ s, we can see a clear difference between equilibrium wave probe values at GM1 and GM3, as expected because of the difference in initial loading condition. One should note that, because we study side damage and beam-sea scenarios, roll motion is seen to be the dominating factor. Roll motion may not always be the most important factor in other damage scenarios. Forward speed effects may also be relevant. Therefore, the presented results are applicable only to the studied scenario.

Greco et al. [49] described an experimental and numerical study on a patrol ship in head-sea waves. They used a simple analysis to estimate the freeboard exceedance and to examine its link with the water-on-deck events. Following their work, we use a simplified calculation of freeboard exceedance and examine its link to flooding occurrence. The freeboard exceedance occurs when the relative vertical motion between the ship model and the local waves has an amplitude larger than the freeboard. If we neglect the local wave elevation associated with radiated and diffracted waves, the relative vertical motion at a position (y,z) can be approximated as in (4)

$$\eta_r = \eta_3 + y\eta_4 - \zeta_w \tag{4}$$

for zero pitch motion. Here ζ_w is the incident wave elevation at y. We have freeboard exceedance on the damage side of the model if

$$\eta_{ra} = \left| \eta_3 - \frac{B}{2}\eta_4 - \zeta_w \right| > h_{fr} \tag{5}$$

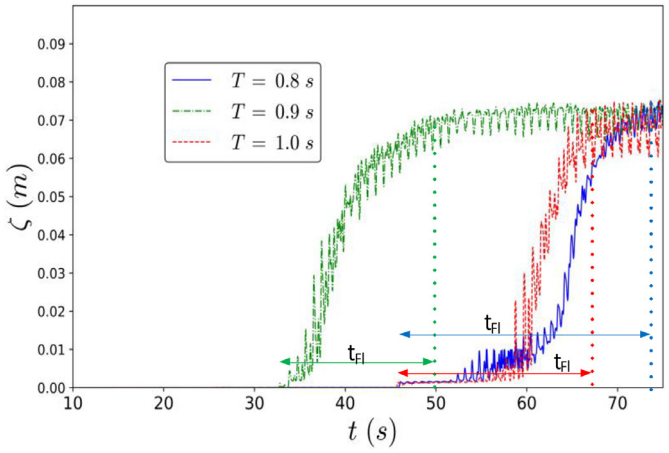

Fig. 35. Wave elevation (WP1) time histories for different time periods, GM3 and steepness kA = 0.066.

with h_{fr} being the damage freeboard. We estimate the relative motion amplitudes from the measurements in the intact test (7 cm draft) in beam waves for kA = 0.033 and assume linear behavior for their calculation at the other two steepnesses. Fig. 37 presents the calculated non-dimensional relative motion parameter, $r = (\eta_{ra} - h_{fr})/h_{fr}$, against the non-dimensional incident wave frequency. The empty symbols represent experimental cases without flooding and full symbols those with flooding. From the figure, the simplified freeboard exceedance, i.e. $r > 0$, corresponds well with the flooding occurrence in most of the examined cases but for few conditions associated with low positive r for which experimentally there is no flooding. This would suggest that for those cases local wave-body interaction matters. Also, the local phase of the wave near the damage could play a role in avoiding the flooding occurrence.

7. Conclusions

Experiments were performed in a wave flume on a thin walled prismatic hull form in 2D flow conditions. The model consists of a damaged rectangular opening located on the side. Freely-floating tests in regular beam-sea waves have been carried out by varying the incident-waves parameters. Effect of damage submergence, damage compartment size, air compressibility in airtight compartment, damage-opening size and initial transient flooding were examined. Video recordings and measurements inside the damage compartment, were performed in all experiments. Motions and internal floodwater heights were measured and analyzed. Test repeatability and main error sources in the tests were discussed. The outcomes of the physical investigations can be summarized as follows:

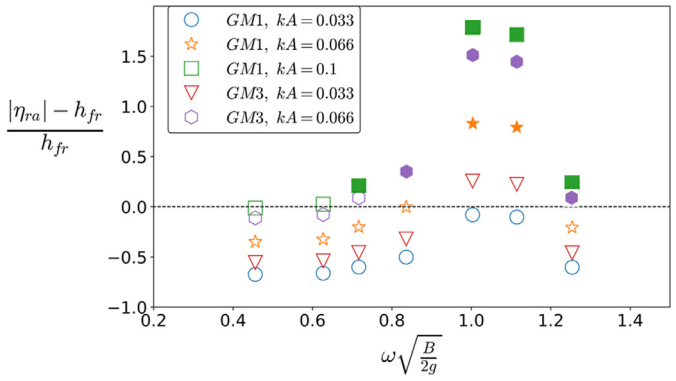

Fig. 37. Non-dimensional flooding parameter as a function of non-dimensional frequency (the solid symbols represent flooding captured in experiments, the empty symbols represent no flooding).

- Free roll decay tests demonstrate that the damage scenario causes a large increase in roll damping and increases also the natural roll resonance period relative to the initial phase. Smaller damage opening decreases the roll damping slightly, whereas for an airtight damaged compartment, the roll damping is highly reduced.
- For a floating damaged section in waves, the floodwater behavior is highly coupled with body motions. The overall behavior is very different as compared to the intact condition. Heave and sway motions are affected to a smaller degree as compared to roll motions. Piston mode and sloshing resonance play an important effect. A linear strip-theory approach, using the CFD solver OpenFOAM, was implemented to estimate alternatively the body motions. The method provided a reasonable agreement with experiments but demonstrated the importance of incorporating nonlinear effects in roll damping for more quantitative comparison at roll resonance.
- Change in initial loading condition modifies the flooding behavior inside the compartment. Since in this case the KG and draft are modified, the natural resonance periods of motions, piston and sloshing mode also shift.
- Air compressibility can have important effects. It slows down the flooding inside the damaged compartment but can excite larger motions in some cases as shown for heave motions. Air compressibility is, however, associated with scale effects with Euler number. Detailed analysis for a single DOF in heave motion is shown in [1].
- Results from present transient-flooding tests show that flooding takes place in beam-sea waves near roll-resonance wave periods. Roll resonance varies with KG of the model section and the roll response is affected by the incident-wave period. Therefore, both KG and wave periods, and thus the ratio between the natural roll period and the incident wave period, have an important influence for a

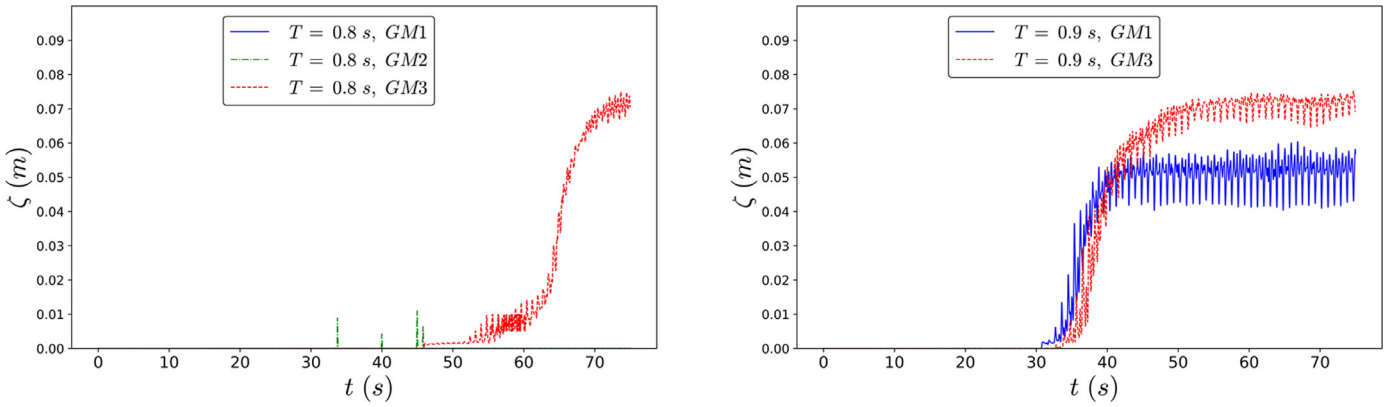

Fig. 36. Wave elevation (WP1) time histories for same time periods and different GMs.

flooding case where damage opening lies above the water surface. Very high wave steepness can also cause flooding even if the wave period is not near roll resonance region. Effect of heave resonance period on transient flooding needs to be studied and is left for future investigations.

- Experimental repeatability is performed for a few cases and is shown to be acceptable (within 20%).

Declaration of Competing Interest

The authors declare that they have no known competing financial interests or personal relationships that could have appeared to influence the work reported in this paper.

Acknowledgement

The authors would like to acknowledge Trond Innset and Torgeir Wahl for their help with experimental setup in the flume. This work has been carried out at the center for Autonomous Marine Operations and Systems (NTNU AMOS). The Research Council of Norway (Norges Forskningsråd) is acknowledged as the main sponsor of NTNU AMOS. This work was supported by the Research Council of Norway through the center of Excellence funding scheme, Project number- 223254 NTNU AMOS.

References

[1] M.A. Siddiqui, M. Greco, O.M. Faltinsen, C. Lugni, Experimental studies of a damaged section in forced heave motion, Applied Ocean Research 88 (2019).
[2] P. Ruponen, Progressive flooding of a damaged passenger ship, PhD Thesis Helsinki University of Technology, 2007.
[3] J.R. Spouge, The technical investigation of the sinking of the Ro-Ro ferry European gateway, Transactions of the Royal Institution of Naval Architects 128 (1986) 49–72.
[4] A. Papanikolaou, G. Zaraphonitis, D. Spanos, E. Boulougouris, E. Eliopoulou, Investigation into the capsizing of damaged ro-ro passenger ships in waves, Proc. 7th Int. Conf. On Stability of Ships and Ocean Vehicles, STAB2000, Tasmania, 2000 Feb. 2000.
[5] D. Spanos, A. Papanikolaou, On the stability of fishing vessels with trapped water on deck, Ship Technology Research 48 (2001) 124–133.
[6] A. Jasionowski, An integrated approach to damage ship survivability assessment, Ph.D. Thesis University of Strathclyde, 2001.
[7] T. Manderbacka, T. Mikkola, P. Ruponen, J. Matusiak, Transient response of a ship to an abrupt flooding accounting for the momentum flux, J Fluids Struct 57 (2015) 108–126.
[8] M. Acanfora, A. Cirillo, A simulation model for ship response in flooding scenario. proceedings of the institution of mechanical engineers, Part M: Journal of Engineering for the Maritime Environment 231 (1) (2017) 153–164.
[9] Q. Gao, D. Vassalos, Numerical study of damage ship hydrodynamics, Ocean Engineering 55 (2012) 199–205.
[10] Z. Gao, Q. Gao, D. Vassalos, Numerical study of damaged ship flooding in beam seas, Ocean Engineering 61 (2013) 77–87.
[11] H. Sadat-Hosseini, D.H. Kim, P.M. Carrica, S.H. Rhee, F. Stern, URANS simulations for a flooded ship in calm water and regular beam waves, Ocean Engineering 120 (2016) 318–330.
[12] H. Hashimoto, K. Kawamura, M. Sueyoshi, A numerical simulation method for transient behavior of damaged ships associated with flooding, Ocean Engineering 143 (2017) 282–294.
[13] E. Begovic, A.H. Day, A. Incecik, S. Mancini, D. Pizzirusso, Roll damping assessment of intact and damaged ship by CFD and EFD methods, Proceedings of the 12th International Conference on the Stability of Ships and Ocean Vehicles, 2015.
[14] A. Papanikolaou, Benchmark study on the capsizing of a damaged ro-ro passenger ship in waves, Technical report, Final report to the 23rd ITTC Specialist Committee on the Prediction of Extreme Motions and Capsizing, 2001.
[15] A. Papanikolaou, D. Spanos, 24th ITTC benchmark study on the numerical prediction of damage ship stability in waves – Preliminary Analysis of results, Proc. 7th Int. Workshop on Stability and Operational Safety of Ships, Shanghai, 2004.
[16] Schindler, M., (2000). Damage stability tests with models of ro-ro ferries – a cost effective method for upgrading and designing ro-ro ferries, contemporary ideas on ship stability, Elsevier.
[17] E. Korkut, M. Altar, A. Incecik, An experimental study of motion behavior with an intact and damaged Ro-Ro ship model, Ocean Engineering 31 (2004) 483–512.
[18] D. Lee, S.Y. Hong, G.J. Lee, Theoretical and experimental study on dynamic behavior of a damaged ship in waves, Ocean Engineering 34 (1) (2007) 21–31.
[19] E. Begovic, G. Mortola, A. Incecik, A.H. Day, Experimental assessment of intact and damaged ship motions in head, beam and quartering seas, Ocean Engineering 72 (1) (2013) 209–226.
[20] S. Lee, J.M. You, H.H. Lee, T. Lim, S.T. Park, J. Seo, S.H. Ree, K.P. Rhee, Experimental study on the six degree-of-freedom motions of a damaged ship floating in regular waves, IEEE Journal of Oceanic Engineering 41 (1) (2015) 40–49.
[21] C. Khaddaj-Mallat, B. Alessandrini, J.M. Rousset, P. Ferrant, An experimental study on the flooding of a damaged passenger ship, Ships and Offshore Structures 7 (1) (2012) 55–71.
[22] T. Manderbacka, P. Ruponen, J. Kulovesi, J.E. Matusiak, Model experiments of the transient response to flooding of the box shaped barge, J Fluids Struct 57 (2015) 127–143.
[23] V.D.K. Domeh, A.J. Sobey, D.A. Hudson, A preliminary experimental investigation into the influence of compartment permeability on damaged ship response in waves, Applied Ocean Research 52 (2015) 27–36.
[24] M. Acanfora, F... De Luca, An experimental investigation into the influence of the damage openings on ship response, Applied Ocean Research 58 (2016) 62–70.
[25] M. Acanfora, F. De Luca, An experimental investigation on the dynamic response of a damaged ship with a realistic arrangement of the flooded compartment, Applied Ocean Research 69 (2017) 191–204.
[26] J. Cichowicz, D. Vassalos, A. Jasionowski, Experiments on a floating body subjected to forced oscillation in calm water at the presence of an open-to-sea compartment, Contemporary Ideas on Ship Stability. Fluid Mechanics and Its Applications 119 (2019).
[27] L. Palazzi, J.O. de Kat, Model experiments and simulations of a damaged ship with airflow taken into account, Marine Technology 41 (1) (2004) 38–44.
[28] P. Ruponen, P. Kurvinen, I. Saisto, J. Harras, Air compression in a flooded tank of a damaged ship, Ocean Engineering 57 (2013) 64–71.
[29] S.S. Bennett, A.B. Phillips, Experimental investigation of the influence of floodwater due to ship grounding on motions and global loads, Ocean Engineering 130 (2017) 49–63.
[30] Y. Gu, A. Day, E. Boulougouris, S. Dai, Experimental investigation on stability of intact and damaged combatant ship in a beam sea, Ships and Offshore Structures 13 (1) (2018) 322–338.
[31] O.M. Faltinsen, A.N. Timokha, Sloshing, Cambridge University Press, 2009.
[32] J. Miles, W. Munk, Harbor paradox, jour. waterways and harbors div. Proc. ASCE 87 (1961) WW3.
[33] B. Molin, On the piston and sloshing modes in moonpools, J Fluid Mech 430 (2001) 27–50.
[34] O.M. Faltinsen, O. Rognebakke, A.N. Timokha, Two-dimensional resonant piston-like sloshing in a moonpool, J Fluid Mech 575 (2007) 359–397.
[35] T. Kristiansen, O.M. Faltinsen, A two-dimensional numerical and experimental study of resonant coupled ship and piston-mode motion, Applied Ocean Research 32 (2) (2010) 158–176.
[36] A.G. Fredriksen, T. Kristiansen, O.M. Faltinsen, Wave-induced response of a floating two-dimensional body with a moonpool, Philos Trans A Math Phys Eng Sci 373 (2033) (2015) Jan 28.
[37] X.J. Kong, O.M. Faltinsen, Piston mode and sloshing resonance in a damaged ship, Proceeding of the 29th International Conference on Ocean, Offshore and Arctic Engineering, 3 2010 OMAE.
[38] J.O. de Kat, Dynamics of a ship with a partially flooded compartment, Contemporary Ideas on Ship Stability, Elsevier Science Ltd, 2000.
[39] E. Begovic, A.H. Day, A. Incecik, An experimental study of hull girder loads on an intact and damaged naval ship, Ocean Engineering 133 (2017) 47–65.
[40] A. Brian, R.L. Pulido, Ship Hydrostatics and Stability, Elsevier Ltd, 2013.
[41] T. Kristiansen, Two-Dimensional numerical and experimental studies of piston-mode resonance, PhD Thesis Norwegian University of Science and Technology, 2009.
[42] O.M. Faltinsen, Hydrodynamics of High-Speed Marine Vehicles, Cambridge University Press, 2005.
[43] N. Salvesen, E.O. Tuck, O.M. Faltinsen, Ship motions and sea loads, The Society of Naval Architects and Marine Engineers. (1970).
[44] Vugts, Ir.J.H., (1968). The hydrodynamic coefficients for swaying, heaving and rolling cylinders in a free surface. Report 112S. Netherlands Ship Research Centre.
[45] O.M. Faltinsen, Sea Loads on Ships and Offshore Structures, Cambridge University Press, 1993.
[46] O.F. Rognebakke, O.M. Faltinsen, Coupling of sloshing and ship motions, Journal of Ship Research 47 (2003) 208–221.
[47] Ypma, E. (2010). Model tests in atmospheric and vacuum conditions, project floodstand (Integrated flooding control and standard for stability and crises management), Deliverable D2.5b, FP7-RTD-218532.
[48] N. Shimizu, R. Kambisseri, Y. Ikeda, An experimental study on flooding into the car deck of a RORO ferry through damaged bow door, Contemporary Ideas on Ship Stability, Elsevier Science Ltd, 2000.
[49] M. Greco, B. Bouscasse, C. Lugni, 3-D seakeeping analysis with water on deck and slamming. part 2: experiments and physical investigation, J Fluids Struct 33 (2012) 148–179.